Research Square

Preprints are preliminary reports that have not undergone peer review.
They should not be considered conclusive, used to inform clinical practice,
or referenced by the media as validated information.

Network Pharmacology and Molecular Docking-Based Investigation of Ricinus communis Aerial-Part Constituents against Dental Pain

Sultan Aati

sati@ksu.edu.sa

King Saud University

Muhammad Ahsan Raza

The Islamia University of Bahawalpur

Kashif-ur-Rehman Khan

The Islamia University of Bahawalpur

Mohammed Alshehri

King Saud University Medical City, King Saud University

Omar Alageel

King Saud University

Obaid Alshahrani

King Saud University

Bilal Ahmad Ghalloo

University of Minnesota

Hanan Aati

King Saud University

Article

Keywords: Ricinus communis, dental pain, pulpitis, network pharmacology, molecular docking, molecular dynamics simulation

Posted Date: November 11th, 2026

DOI: https://doi.org/10.21203/rs.3.rs-11231566/v1

License: This work is licensed under a Creative Commons Attribution 4.0 International License.
Read Full License

Additional Declarations: No competing interests reported.

Network Pharmacology and Molecular Docking-Based Investigation of *Ricinus communis* Aerial-Part Constituents against Dental Pain

Sultan Aati[1]*, Muhammad Ahsan Raza[2]*, Kashif-ur-Rehman Khan[3], Mohammed Alshehri[4], Omar Alageel[1], Obaid Alshahrani[1], Bilal Ahmad Ghalloo[5], Hanan Aati[6]

1. Dental Health Department, College of Applied Medical Sciences, King Saud University, Riyadh, Saudi Arabia.
2. Faculty of Pharmacy, The Islamia University of Bahawalpur 63100, Bahawalpur, Pakistan.
3. Department of Pharmaceutical Chemistry, Faculty of Pharmacy, The Islamia University of Bahawalpur 63100, Bahawalpur, Pakistan.
4. Center of Excellence in Biotechnology Research, King Saud University Medical City, King Saud University, Riyadh, Saudi Arabia
5. Department of Medicinal Chemistry, College of Pharmacy, University of Minnesota, Minneapolis, MN 55454, USA.
6. Department of Pharmacognosy, College of Pharmacy, King Saud University, Riyadh 11495, Saudi Arabia

Kashif-ur-Rehman Khan
Kashifur.rahman@iub.com

Mohammed Alshehri
Mohaalshehri@ksu.edu.sa

Omar Alageel
oalageel@ksu.edu.sa

Obaid Alshahrani
oalshahrani@ksu.edu.sa

Bilal Ahmad Ghalloo
Drbilal29@hotmail.com

Hanan Aati
hati@ksu.edu.sa

***Corresponding author**
Sultan Aati
sati@ksu.edu.sa

Muhammad Ahsan Raza
muhammadahsanraza922@gmail.com
https://orcid.org/0009-0000-4397-3927

Running Head

***Ricinus communis* in Dental Pain**

Abstract

Dental pain associated with pulpitis and odontogenic inflammation remains a common clinical problem, while currently used analgesics can cause adverse effects that limit their use. *Ricinus communis* L. has traditionally been used for painful and inflammatory conditions, but its potential molecular basis in dental pain remains poorly understood. Here, we used an integrated computational pharmacology workflow to investigate the potential mechanisms of *R. communis* phytoconstituents. 47 phytochemicals were screened for ADME, drug-likeness, and toxicity profiles, resulting in three prioritized compounds; i.e. 3,4-dimethoxy-6,8-dihydroxycoumarin, ferulic acid and p-coumaric acid. Target prediction and intersection with 1,909 dental pain associated genes identified 55 common targets. Protein-protein interaction and centrality analyses highlighted PTGS2, NFKB1, MMP9, STAT3 and EGFR as key network targets. Enrichment and pathway analyses indicated involvement of IL-17, PI3K-AKT, and HIF-1 signaling. Molecular docking showed favorable predicted interactions of the prioritized compounds with the selected targets, while 25 ns molecular dynamics simulations indicated overall stability of the corresponding complexes. Together, these findings suggest that *R. communis* phytoconstituents may influence interconnected inflammatory and nociceptive pathways and identify candidate compounds and targets for experimental investigation in dental pain.

Keywords: *Ricinus communis*; dental pain; pulpitis; network pharmacology; molecular docking; molecular dynamics simulation

1. Introductions

Dental pain is among the most common reasons patients seek emergency and routine dental care worldwide, most often arising from pulpitis, periapical inflammation, and periodontal disease. Global Burden of Disease data indicate that oral conditions collectively affect nearly half of the world's population, with untreated caries the principal precursor of pulpal inflammation and dental pain remaining one of the most prevalent health conditions globally and projected to rise further by 2050 [1, 2]. Beyond the direct clinical burden, dental pain imposes substantial indirect costs through school and work absenteeism, reduced quality of life, and downstream healthcare expenditure, particularly in low- and middle-resource settings with limited access to timely dental care [3].

Current pharmacological management of dental pain relies predominantly on non-steroidal anti-inflammatory drugs (NSAIDs) and, in more severe cases, opioid analgesics. NSAIDs are generally recommended as first-line therapy because they act directly on the cyclooxygenase-mediated prostaglandin synthesis responsible for post-procedural inflammation, swelling, and hyperalgesia [4]. However, their use is constrained by dose-dependent gastrointestinal and renal adverse effects, which are estimated to cause over 100,000 hospitalizations annually in the United States alone [5]. Opioids, although effective for severe pain, primarily modulate nociceptive pain transmission and do not address the underlying inflammatory process. Their use is further limited by adverse effects and the risks of misuse, tolerance, dependence, and opioid use disorder. Consequently, contemporary dental guidelines recommend non-opioid analgesics, particularly NSAIDs alone or in combination with acetaminophen, as first-line therapy for acute dental pain, reserving opioids for situations in which first-line treatment is inadequate or contraindicated [6]. These limitations underscore a continued need for alternative

or adjunct therapeutic agents that can target the underlying inflammatory-nociceptive pathways of dental pain with an improved safety profile.

Medicinal plants have long served as a reservoir of bioactive compounds for pain and inflammation, and *Ricinus communis* L. (Euphorbiaceae), commonly known as the castor plant, is one such species with an extensive history of traditional use. Various parts of *R. communis* including its leaves, roots, and seed oil have been traditionally used to manage inflammatory conditions, wounds, and pain across multiple traditional medicine systems [7]. Phytochemical investigations of *Ricinus communis* L. have revealed a diverse array of bioactive constituents, including alkaloids, flavonoids, coumarins, terpenoids, sterols, phenolic compounds, and fatty acids. Despite this phytochemical diversity and reported pharmacological potential, the analgesic and anti-inflammatory properties of *R. communis* remain insufficiently characterized in relation to specific experimental models and mechanisms of action [8]. Despite the available ethnopharmacological and phytochemical evidence, the molecular targets and signaling pathways underlying the potential analgesic and anti-inflammatory effects of *Ricinus communis* L. in dental pain remain poorly characterized. Although diverse phytoconstituents and pharmacological activities have been reported for *R. communis*, the specific molecular interactions relevant to inflammatory and nociceptive processes associated with pulpitis and odontogenic pain remain insufficiently explored [9].

Network pharmacology provides a useful systems-level approach for investigating multi-component medicinal plants by integrating compound-target prediction, disease-associated targets, protein-protein interaction (PPI) networks, and pathway enrichment. This framework is particularly suitable for natural products because their biological effects may arise from the combined actions of multiple constituents on interconnected molecular targets and pathways rather than through a single target [10]. These predictions can be further examined using structure-based approaches. Molecular docking enables the prediction of ligand-binding poses and interaction profiles within candidate protein targets, whereas molecular dynamics (MD) simulation can provide additional information on the conformational stability and persistence of predicted protein–ligand complexes over time [11]. Together, these approaches can strengthen the structural interpretation of network-based target predictions, although experimental studies are ultimately required to confirm biological target engagement.

In the present study, we employed an integrated *in silico* workflow comprising phytochemical curation, sequential ADME and toxicity screening, network pharmacology, density functional theory (DFT)-based geometry optimization, molecular docking, and molecular dynamics simulation to investigate the potential molecular basis of *R. communis* activity against dental pain. The study aimed to identify candidate inflammatory and nociceptive targets and associated signaling pathways and to characterize the most promising phytoconstituent-target interactions using complementary structure-based approaches.

2. Results

2.1 Phytochemical profiling and compound curation

A total of 47 phytochemicals reported from the aerial parts of *Ricinus communis* were compiled from the selected databases. The compounds belonged to several chemical groups, including phenolics, flavonoids, fatty acids, terpenoids, sterols, and organic acids. The structures were then checked and duplicate entries were removed to obtain a non-redundant compound set.

2.2 Sequential screening of phytoconstituents

The initial SwissADME screening of the 47 unique *R. communis* phytochemicals resulted in 24 compounds meeting the selected criteria of bioavailability score ≥0.55, no Lipinski violations, and high GI absorption (Supplementary Table S1). These compounds were further assessed using ADMETlab 3.0, where a DL score >0.65 was used as the cutoff (Supplementary Table S2).

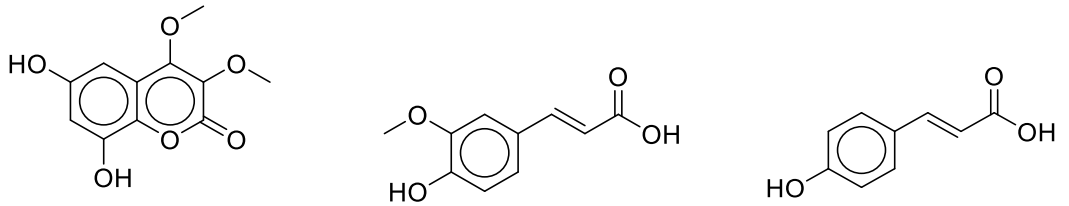
Three compounds met this criterion: 3,4-dimethoxy-6,8-dihydroxycoumarin, ferulic acid, and p-coumaric acid. Their bioavailability scores were 0.55, 0.85, and 0.85, respectively, while their Drug likiness values were 0.764, 0.715, and 0.651. All three showed high GI absorption and no Lipinski violations (Table 1). ProTox 3.0 predicted toxicity classes 5, 4, and 5 for 3,4-dimethoxy-6,8-dihydroxycoumarin, ferulic acid, and p-coumaric acid, respectively. All three compounds were retained for the subsequent target prediction and network pharmacology analyses (Supplementary Table S3).

Table 1. *In silico* ADME, drug-likeness, and toxicity profiles of the four prioritized *Ricinus communis* phytoconstituents.

Compound name	GI absorption	Lipinski violations	Bioavailability score	DL score	Toxicity class
3,4-Dimethoxy-6,8-dihydroxycoumarin	High	0	0.55	0.764	5
Ferulic acid	High	0	0.85	0.715	4
p-Coumaric acid	High	0	0.85	0.651	5

Toxicity Class I: fatal if swallowed (LD50 ≤ 5), Class II: fatal if swallowed (5 < LD50 ≤ 50), Class III: toxic if swallowed (50 < LD50 ≤ 300), Class IV: harmful if swallowed (300 < LD50 ≤ 2000), Class V: may be harmful if swallowed (2000 < LD50 ≤ 5000), Class VI: non-toxic (LD50 > 5000)

Molecular Weight (MW); Gastrointestinal (GI); Drug Likiness (DL)



(1) (2) (3)

Figure 1. Chemical structures of the prioritized compounds identified in *Ricinus communis*: **(1)** 3,4-Dimethoxy-6,8-dihydroxycoumarin, **(2)** Ferulic acid, and **(3)** p-Coumaric acid

2.3. Common Targets between Dental Pain and Prioritized *R. communis* Phytoconstituents

Dental pain related targets were identified from GeneCards and CTD using the terms "Pulpitis" and "Toothache." GeneCards identified 303 targets for pulpitis and 461 for toothache, whereas CTD identified 8,374 and 931 targets, respectively. After applying the predefined selection criteria and removing duplicate entries, 1,909 unique dental pain-related targets were obtained. Target prediction for the three prioritized *R. communis* phytoconstituents identified 100 targets for each compound. Combining the three target lists and removing duplicates resulted in 171 unique targets. Comparison of the two datasets identified 55 targets common to both the prioritized phytoconstituents and dental pain (Figure 2). These common targets were used for the subsequent PPI network and enrichment analyses.

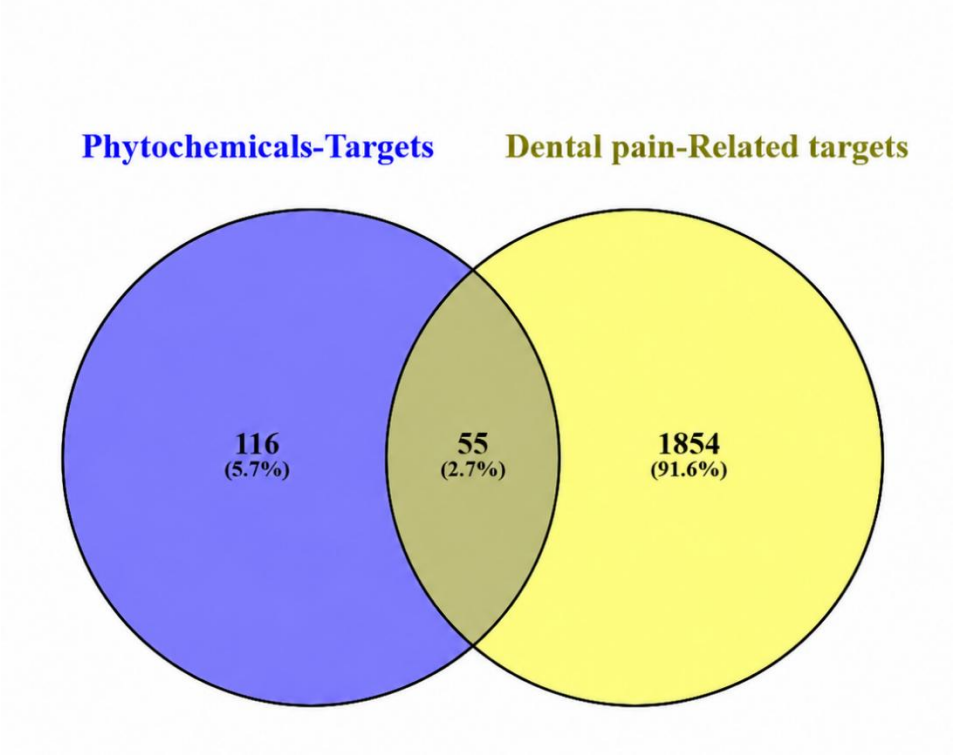


Figure 2. Venn diagram showing the intersection of targets associated with dental pain and prioritized compounds.

2.4. Protein-Protein Interaction (PPI) Network Construction and Hub Gene Prediction

The 55 common targets were analyzed using STRING, generating a PPI network comprising 55 nodes and 401 edges. The network showed an average node degree of 14.6, with an average local clustering coefficient of 0.635. The observed number of interactions was higher than expected (401 observed vs. 135 expected edges; PPI enrichment $p<1\times10^{-16}$), indicating significant connectivity among the common targets (Figure 3).

The network was further analyzed using the CytoHubba plugin in Cytoscape with the Maximal Clique Centrality (MCC) method. The five highest ranked targets were PTGS2, NFKB1, MMP9, STAT3 and EGFR (Figure 4). These targets were selected as hub genes and were subsequently used for molecular docking analysis.

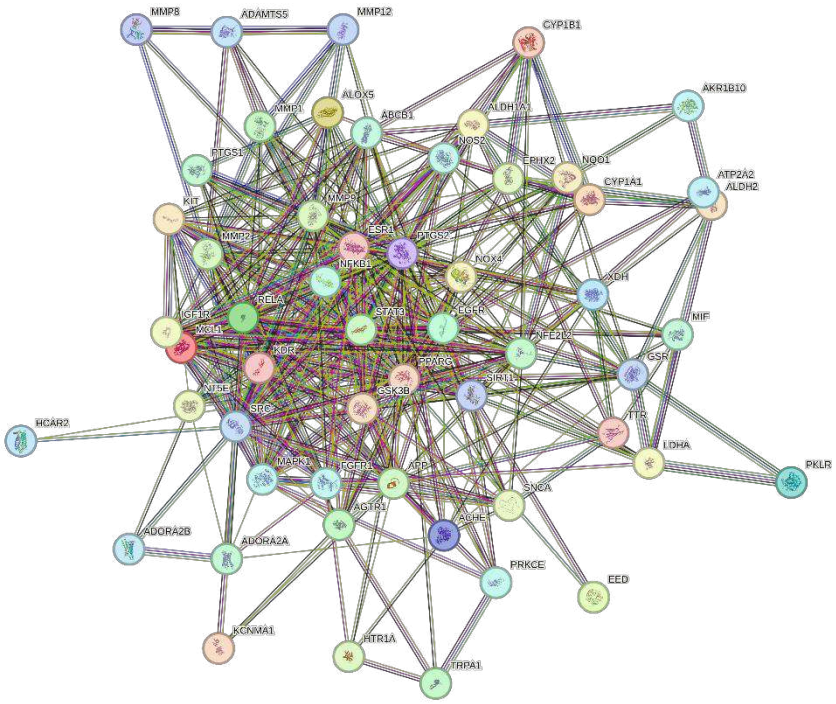


Figure 3. PPI network and hub gene identification. The PPI network consisted of 55 common targets with 401 interactions.

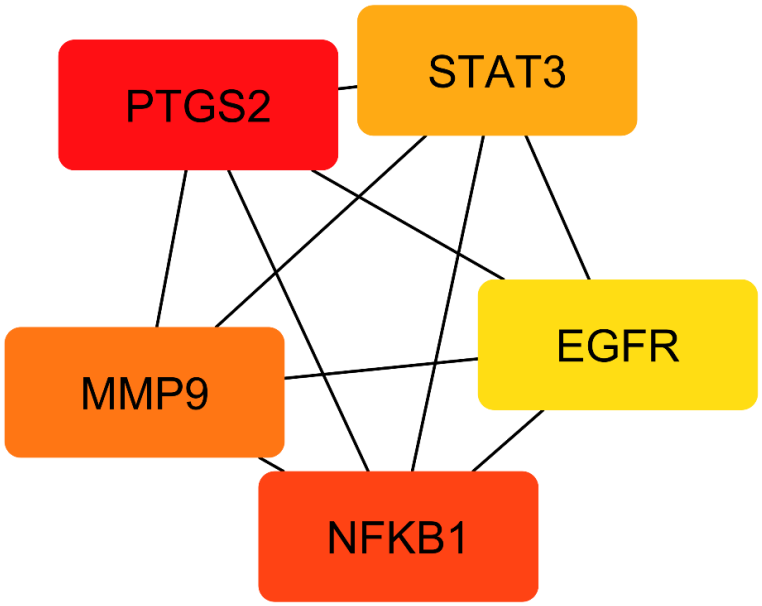


Figure 4. Hub genes identified from the PPI network using the MCC algorithm. The five topranked hub genes were PTGS2, NFKB1, MMP9, STAT3 and EGFR.

2.5. Gene Ontology and KEGG Pathway Enrichment Analysis

GO enrichment analysis of the 55 common targets showed a pattern closely related to the inflammatory and neural features of dental pain (Figure 5A). In the Biological Process category, the strongest enrichment was observed for cellular and general responses to oxidative and chemical stress, together with inflammatory response and regulation of cellular signaling (Figure 5B). Cellular response (Figure 5C) to oxidative stress showed the highest fold enrichment (~21-fold), followed by cellular response to chemical stress (~20-fold) and response to oxidative stress (~17-fold). The Cellular Component analysis extended this pattern to membrane and neuronal structures, with enrichment of membrane rafts, caveolae, glutamatergic synapses, neuronal cell bodies, axons, and other synaptic compartments. These findings are relevant to dental pain because the dental pulp is densely innervated, and changes within the inflamed pulp can interact with sensory nerve activity and pain transmission.

The Molecular Function analysis further showed enrichment of receptor tyrosine kinase and other kinase-related activities, together with oxidoreductase and transcription factor-associated functions. This indicates that the common targets are involved not only in inflammatory responses but also in signaling processes capable of linking extracellular stimuli to intracellular cellular responses (Figure 5D). KEGG analysis supported this relationship. Several signaling pathways associated with inflammatory and cellular stress responses were significantly enriched, including the IL-17, HIF-1, PI3K-Akt, Ras, and calcium signaling pathways. The IL-17 pathway is consistent with the inflammatory component of pulpitis, whereas HIF-1 signaling is relevant to the hypoxic and inflammatory environment of the dental pulp. PI3K-Akt and Ras signaling provide additional links between receptor-mediated stimulation and intracellular responses.

Taken together, the GO and KEGG findings placed the 55 common targets within a connected biological framework involving oxidative stress, inflammation, cellular signaling, and neuronal function. Rather than pointing to a single pathway, the results suggest that the prioritized *R. communis* phytoconstituents are associated with multiple interconnected processes that are relevant to the development and transmission of dental pain. This interpretation is consistent with the current understanding of pulpitis as a condition in which inflammatory, vascular, and neural responses interact to promote nociception and sensitization.

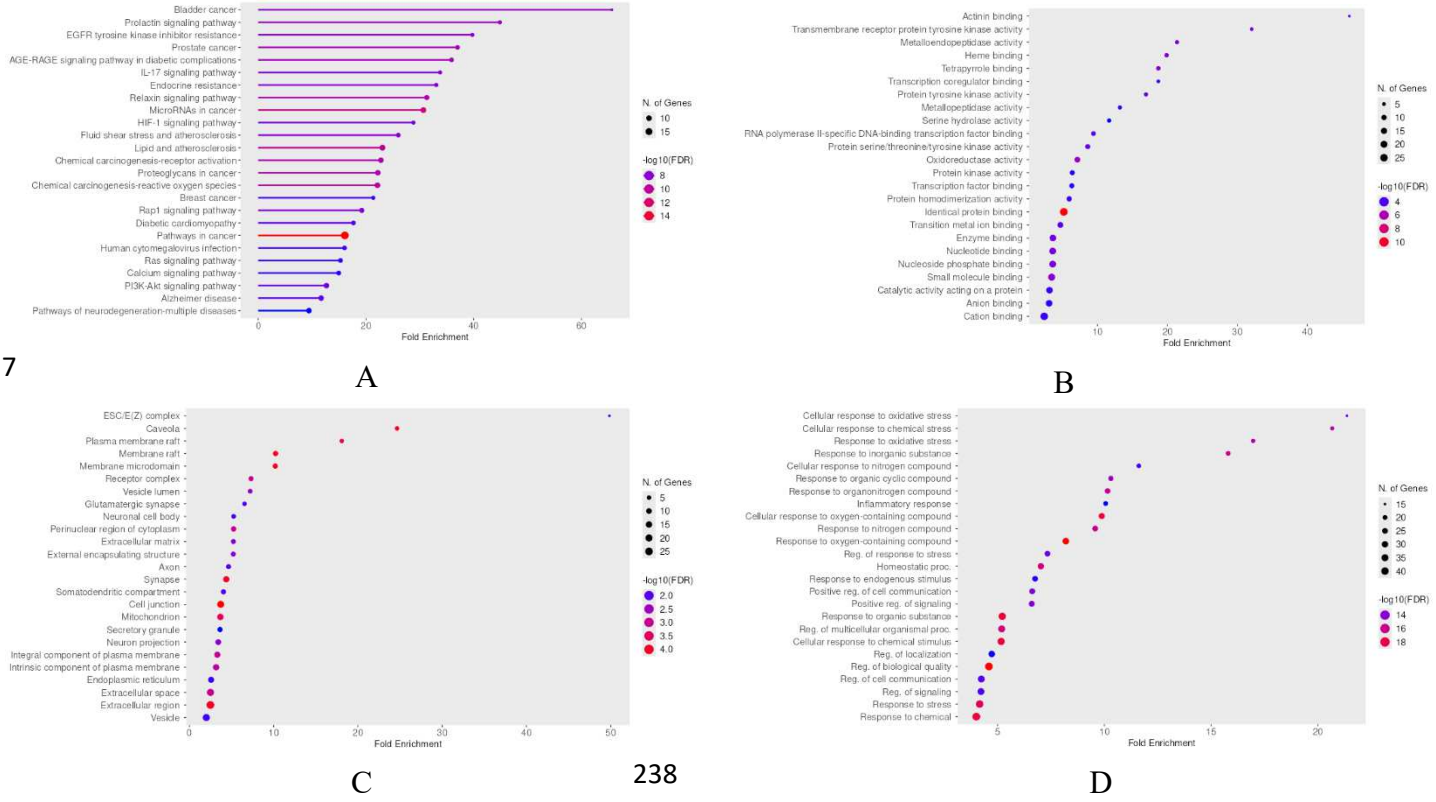


Figure 5. Gene Ontology and KEGG pathway enrichment analysis of the common targets. **(A)** KEGG pathway enrichment analysis showing the significantly enriched pathways associated with the common targets, **(B)** Biological Process (BP) enrichment analysis **(C)** Cellular Component (CC) enrichment analysis and **(D)** Molecular Function (MF) enrichment analysis

2.6. KEGG Pathway Mapping of Target Genes

To contextualize the mechanistic relevance of the five top ranked hub targets; i.e. PTGS2, NFKB1, MMP9, STAT3, and EGFR the target network was subjected to KEGG pathway enrichment analysis, and the highest ranked, functionally converging pathways were visualized using Pathview. Three pathways emerged as the most biologically informative with respect to nociceptive and inflammatory signaling relevant to dental pain; e.g. the IL-17 signaling pathway, the PI3K-AKT signaling pathway, and the HIF-1 signaling pathway (Figures 6A-6B). In each diagram, nodes corresponding to genes present in the *Ricinus communis*-dental pain target network are highlighted in red, and their distribution across the three maps indicates convergent signaling rather than isolated, pathway-specific effects.

In the IL-17 signaling pathway (Figure 6A), NF-κB (NFKB1) appeared as a shared downstream node across the IL-17A/F, IL-17B, and IL-17C branches, together with MAPK3/ERK, GSK3β, and the matrix metalloproteinases MMP1 and MMP9, which feed into chemokine, cytokine, and tissue-remodeling outputs. In the PI3K-AKT signaling pathway (Figure 6B), the receptor tyrosine kinase (RTK) node representing EGFR family input together with ERK, GSK3, NF-κB, and the anti-apoptotic effector Mcl-1, were highlighted downstream of growth factor receptor activation, linking receptor signaling to cell survival and proliferative outputs. In the

HIF-1 signaling pathway (Figure 6C), RTK, ERK, STAT3, NF-κB, iNOS, and LDHA were highlighted, reflecting convergence of hypoxia-responsive and inflammatory transcriptional programs.

Collectively, NF-κB, ERK, and RTK/EGFR-linked nodes recur across all three pathways, positioning them as central hubs through which the network target genes exert coordinated effects on inflammatory mediator production, tissue remodeling, and cell survival/proliferative signaling processes mechanistically linked to pulpal and periodontal nociception.

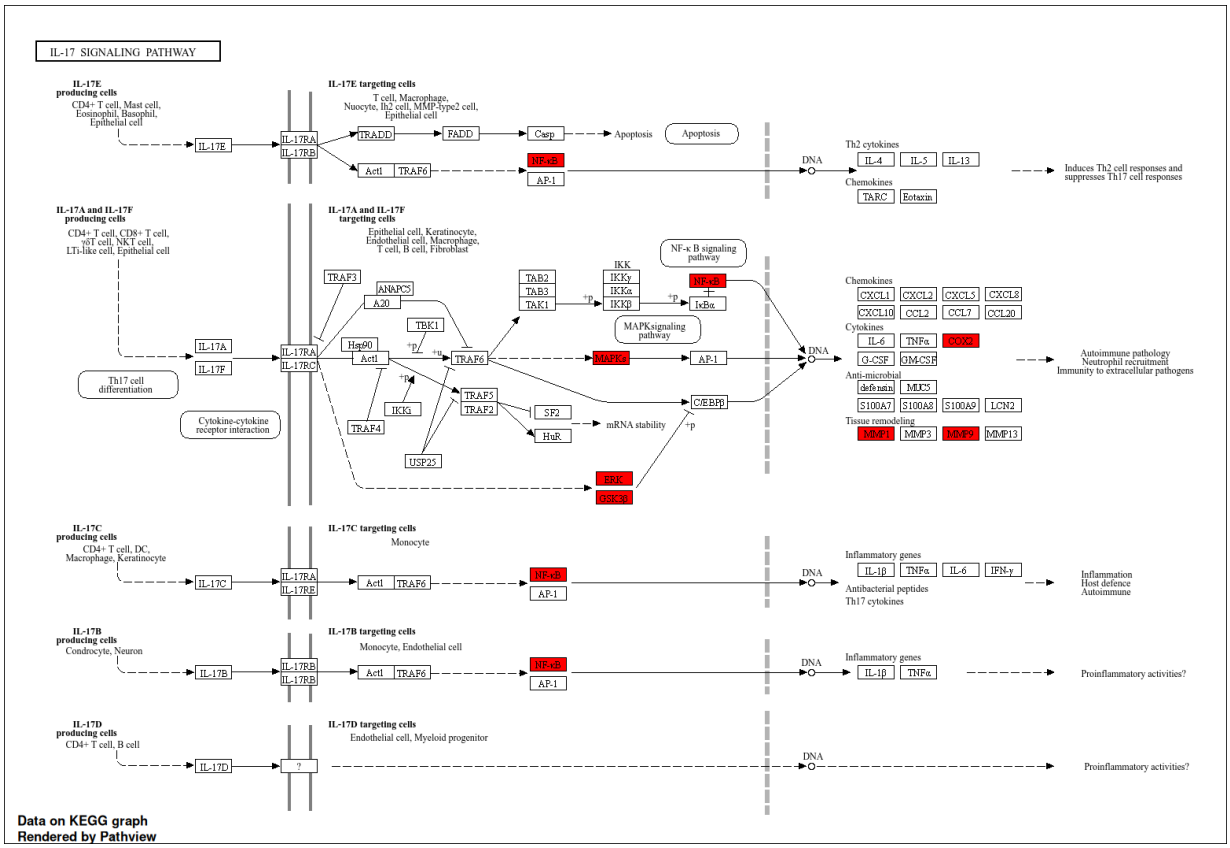


Figure 6A. KEGG based visualization of the IL-17 signaling pathway (hsa04657) showing predicted targets of *Ricinus communis* phytoconstituents. Pathway map generated using Pathview, with nodes highlighted in red indicating hub/network target genes identified through the network pharmacology analysis (NF-κB, MAPK3/ERK, GSK3β, CXCL2, MMP1, and MMP9). This figure was generated using the KEGG PATHWAY database with permission from Kanehisa Laboratories [12].

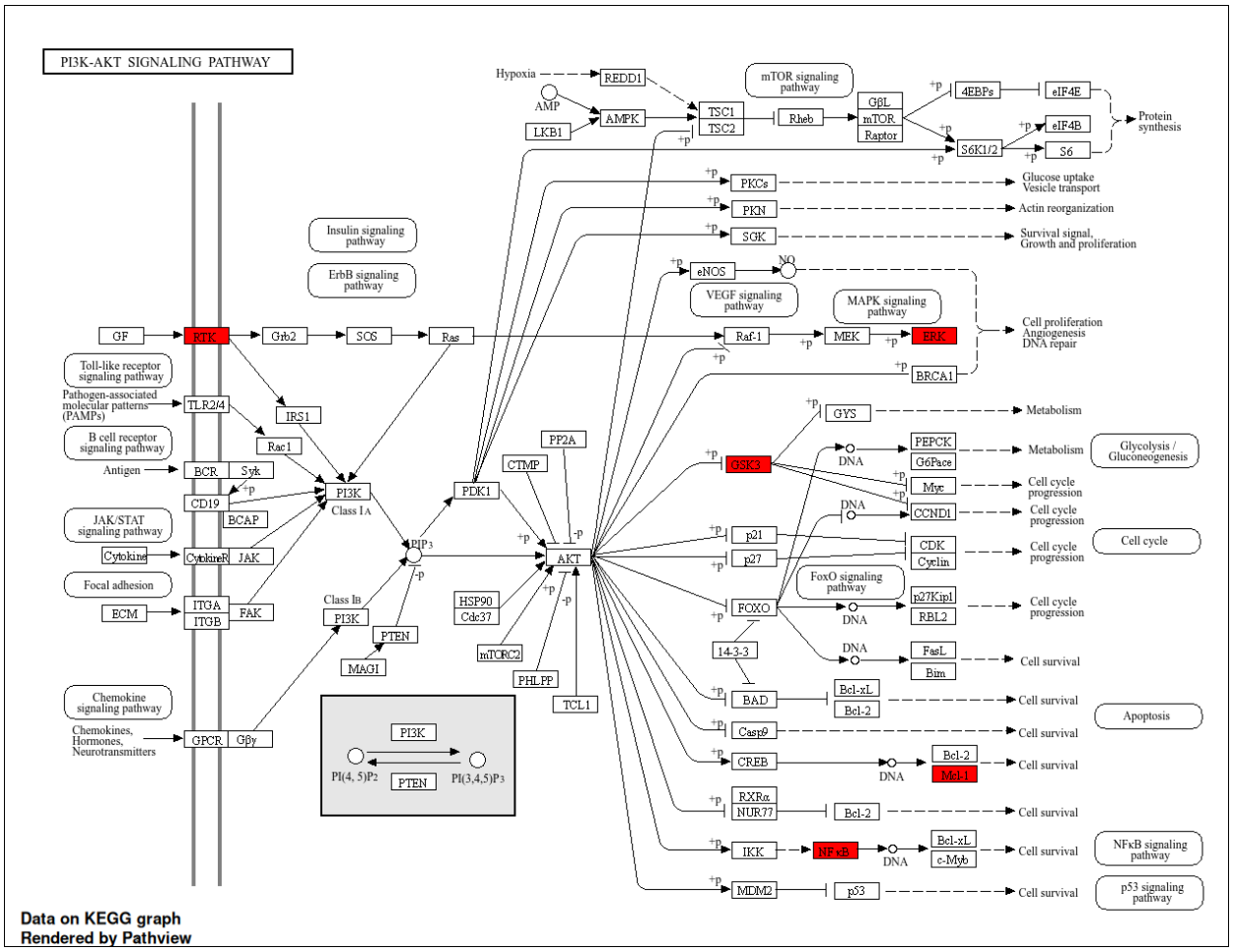


Figure 6B. KEGG-based visualization of the PI3K-AKT signaling pathway (hsa04151) showing predicted targets of *Ricinus communis* phytoconstituents. Pathway map generated using Pathview, with red nodes denoting network hub genes (RTK, ERK, GSK3, NF-κB, and Mcl-1) mapped onto the reference pathway. This figure was generated using the KEGG PATHWAY database with permission from Kanehisa Laboratories [13].

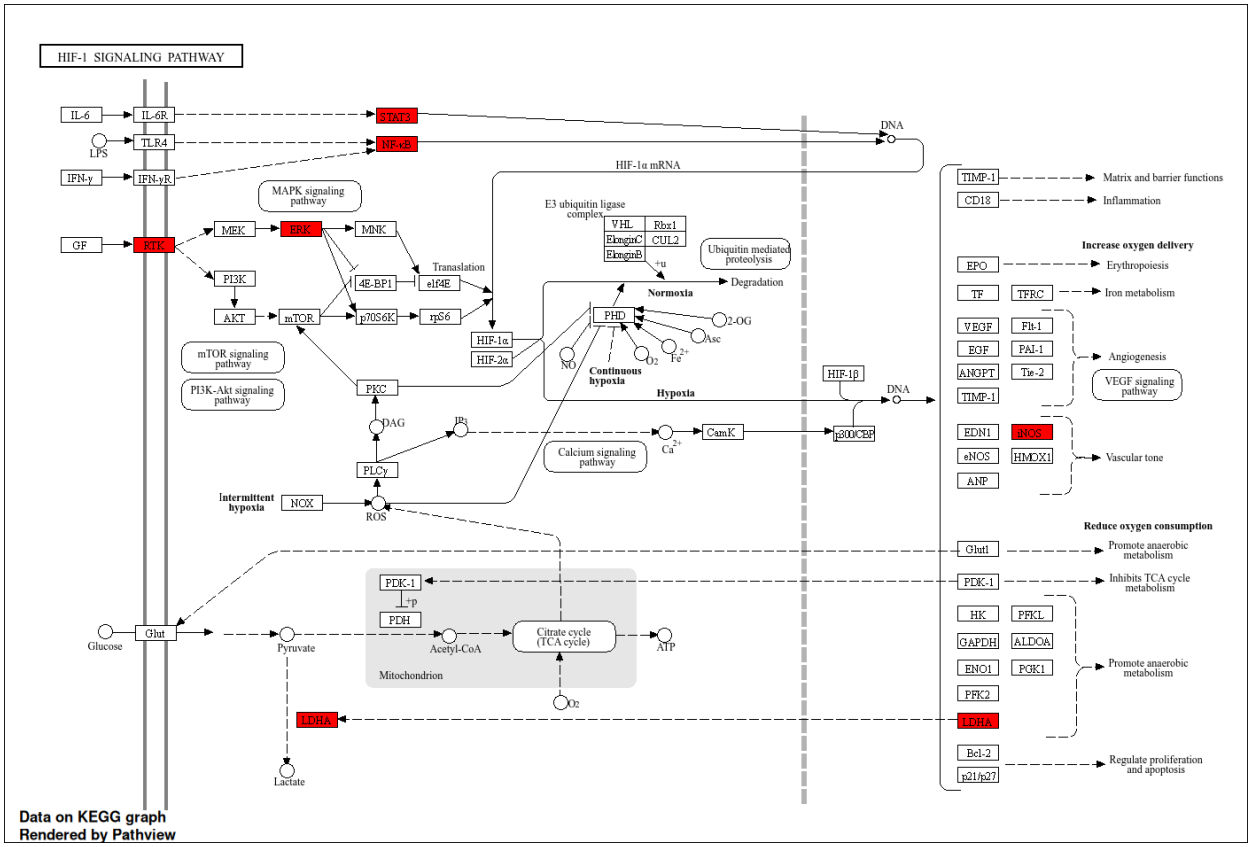


Figure 6C. KEGG-based visualization of the HIF-1 signaling pathway (hsa04066) showing predicted targets of *Ricinus communis* phytoconstituents. Pathway map generated using Pathview, with red nodes indicating network hub genes (RTK, ERK, STAT3, NF-κB, iNOS, and LDHA) overlaid on the reference pathway. This figure was generated using the KEGG PATHWAY database with permission from Kanehisa Laboratories [12, 14].

2.7. Compound target pathway network

To visualize the polypharmacological basis of *Ricinus communis* against dental pain, a compound target pathway network was constructed in Cytoscape by integrating the three bioactive constituents (ferulic acid, p-coumaric acid, and 3,4-dimethoxy-6,8-dihydroxy-coumarin) with their predicted gene targets and the corresponding enriched KEGG pathways (Figure 7). The resulting network comprised 64 nodes 3 compound nodes, 55 target-gene nodes, and 6 pathway nodes connected by a dense edge set reflecting extensive one-to-many and many-to-many compound target and target pathway relationships.

All three compounds shared a substantial overlapping target pool, indicating that the observed pharmacological activity of *Ricinus communis* is unlikely to be attributable to a single constituent but instead arises from the combined, convergent action of multiple phytochemicals on a shared target repertoire a hallmark of network pharmacology based herbal activity.

Among the 55 target genes, 22 (MMP1, MMP2, MMP9, KIT, NOS2, IGF1R, AGTR1, FGFR1, PTGS2, ADORA2A, ADORA2B, KDR, STAT3, MCL1, NOX4, GSK3B, MAPK1, ATP2A2, EGFR, PRKCE, RELA, and NFKB1) mapped directly onto one or more of the six significantly enriched KEGG pathways; i.e. Calcium signaling, IL-17 signaling, Ras signaling, PI3K-AKT

signaling, HIF-1 signaling, and AGE-RAGE signaling in diabetic complications. The remaining 33 targets did not map onto these six pathways but were retained in the network as compound-associated targets supported by the underlying protein–protein interaction and target-prediction data. Within the pathway linked target subset, RELA, NFKB1, MAPK1, STAT3, and EGFR emerged as the most highly connected nodes, each linking to multiple pathway nodes simultaneously, positioning them as convergence point through which several signaling cascades intersect. Notably, this pathway mapped hub set overlaps substantially with the top ranked hub genes identified independently through the protein-protein interaction network analysis (PTGS2, NFKB1, MMP9, STAT3, and EGFR), providing cross validation between the two analytical approaches.

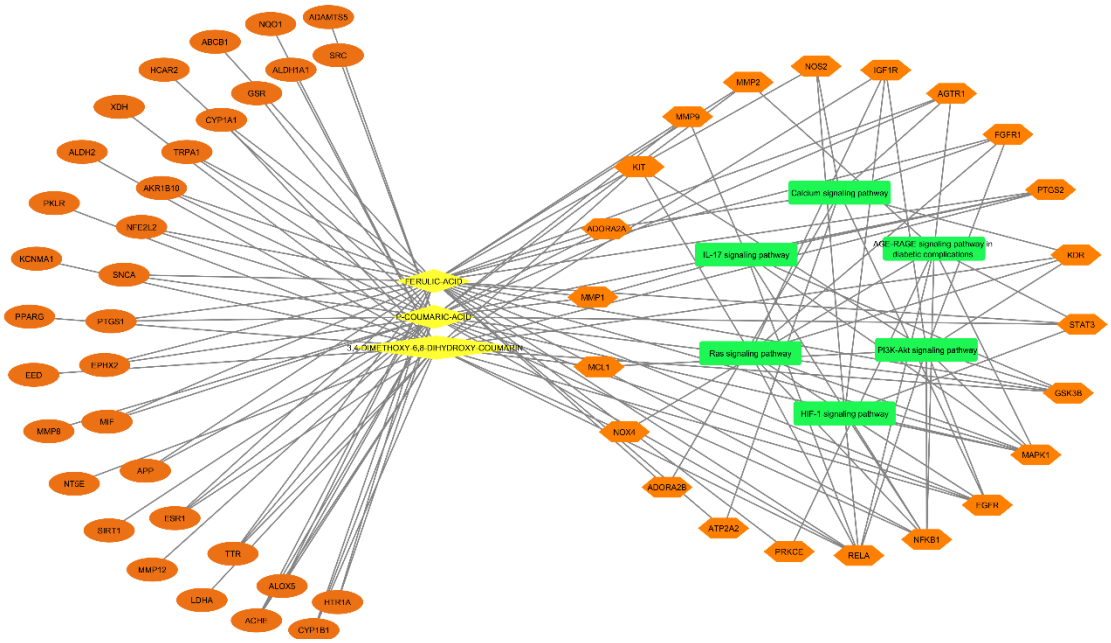


Figure 7. Compound target pathway network of the bioactive constituents of *Ricinus communis* against dental pain targets. Network constructed and visualized in Cytoscape. Yellow diamond nodes represent the three bioactive compounds (ferulic acid, p-coumaric acid, and 3,4-dimethoxy-6,8-dihydroxy-coumarin); orange nodes represent their predicted gene targets, with hexagonal nodes denoting targets that map onto one or more enriched KEGG pathways and elliptical nodes denoting targets without direct pathway mapping in this network; green rectangular nodes represent the significantly enriched KEGG signaling pathways (Calcium signaling, IL-17 signaling, Ras signaling, PI3K-AKT signaling, HIF-1 signaling, and AGE-RAGE signaling in diabetic complications). Edges connect each compound to its predicted targets and each target to its associated pathway(s), illustrating the multi-compound, multi-target, multi-pathway pharmacological basis of *Ricinus communis* against dental pain.

2.8. Density functional theory based geometry optimization

Geometry optimization was performed at the B3LYP/6-311G level to obtain optimized three-dimensional structures of the selected *Ricinus communis* phytochemicals for subsequent molecular docking analysis. The optimized structures and their corresponding frontier molecular orbitals are presented in Figure 8. The HOMO and LUMO were mainly distributed

over the conjugated regions and oxygen-containing functional groups, with some differences in their distribution among the compounds. The optimized compounds showed differences in their frontier orbital energies and related electronic descriptors (Table 2). The HOMO-LUMO energy gaps were 4.0964 eV for 3,4-dimethoxy-6,8-dihydroxycoumarin, 4.1869 eV for ferulic acid, and 4.2558 eV for p-coumaric acid. Among the three compounds, 3,4-dimethoxy-6,8-dihydroxycoumarin showed the smallest energy gap, together with the lowest chemical hardness (2.0482 eV) and highest softness (0.4882 eV^{-1}). Ferulic acid showed intermediate values, whereas p-coumaric acid had the largest energy gap (4.2558 eV), highest hardness (2.1279 eV), and lowest softness (0.4699 eV^{-1}).

The calculated HOMO energies were −6.049, −6.293, and −6.3837 eV, while the corresponding LUMO energies were −1.9526, −2.1061, and −2.1279 eV for 3,4-dimethoxy-6,8-dihydroxycoumarin, ferulic acid, and p-coumaric acid, respectively. Other CDFT descriptors, including ionization potential, electron affinity, chemical potential, electronegativity, and electrophilicity index, are summarized in Table 2. Overall, DFT optimization provided energetically optimized ligand geometries for the subsequent molecular docking studies. The calculated electronic descriptors further characterized the electronic nature of the selected compounds and supported their use as optimized structures for docking-based evaluation of their interactions with the selected targets.

Table 2. DFT-calculated frontier molecular orbital energies and conceptual density functional theory (CDFT) descriptors of the selected *Ricinus communis* phytochemicals.

CDFT descriptors (eV)	3,4-Dimethoxy-6,8-dihydroxycoumarin	Ferulic acid	p-Coumaric acid
E_{LUMO}	-1.9526	-2.1061	-2.1279
E_{HOMO}	-6.049	-6.293	-6.3837
Energy gap	4.0964	4.1869	4.2558
Ionization Energy	6.049	6.293	6.3837
Electron affinity	1.9526	2.1061	2.1279
Hardness	2.0482	2.0934	2.1279
Softness	0.4882	0.4776	0.4699
Electronegativity	4.0008	4.1995	4.2558
Chemical potential	-4.0008	-4.1995	-4.2558
Electrophilicity index	3.9078	4.2122	4.2557

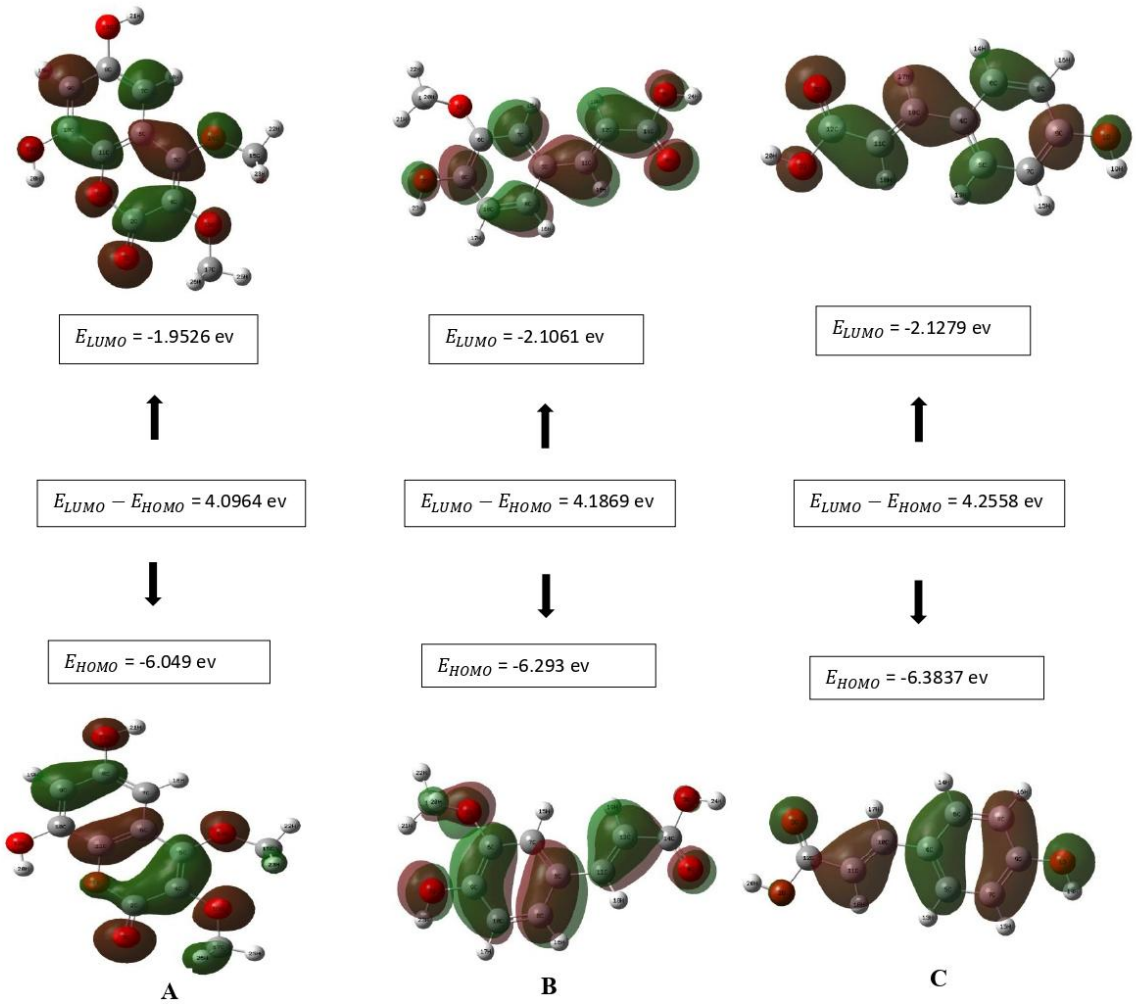


Figure 8. DFT-optimized molecular structures and corresponding HOMO and LUMO distributions of the selected *Ricinus communis* phytochemicals. **(A)** 3,4-dimethoxy-6,8-dihydroxycoumarin, **(B)** ferulic acid, and **(C)** p-coumaric acid.

2.9. Molecular docking analysis

Molecular docking was carried out to assess the binding affinity of 3,4-dimethoxy-6,8-dihydroxycoumarin, ferulic acid, and p-coumaric acid toward PTGS2, NFKB1, MMP9, STAT3, and EGFR. The predicted binding energies are summarized in Table 3. All compounds exhibited negative docking scores across the selected targets, with differences in their predicted binding affinities. 3,4-Dimethoxy-6,8-dihydroxycoumarin showed the lowest binding energy toward PTGS2 (−7.1 kcal/mol), followed by ferulic acid (−6.8 kcal/mol) and p-coumaric acid (−6.4 kcal/mol). A similar pattern was observed for NFKB1, where 3,4-dimethoxy-6,8-dihydroxycoumarin showed the lowest binding energy (−5.5 kcal/mol), compared with ferulic acid (−4.9 kcal/mol) and p-coumaric acid (−4.8 kcal/mol). For EGFR, the corresponding docking scores were −6.8, −6.4, and −6.0 kcal/mol, respectively. In contrast, ferulic acid showed the lowest binding energy toward MMP9 (−7.9 kcal/mol), followed by p-coumaric acid (−7.6 kcal/mol) and 3,4-dimethoxy-6,8-dihydroxycoumarin (−6.6 kcal/mol). The three compounds displayed relatively close docking scores against STAT3, ranging from −4.2 to −4.5 kcal/mol. The lowest score was observed for 3,4-dimethoxy-6,8-dihydroxycoumarin (−4.5 kcal/mol), followed by ferulic acid (−4.4 kcal/mol) and p-coumaric acid (−4.2 kcal/mol). Overall, 3,4-dimethoxy-6,8-dihydroxycoumarin exhibited the most favorable predicted binding scores against four of the five investigated targets, namely PTGS2, NFKB1, STAT3, and EGFR, whereas ferulic acid showed the strongest predicted binding toward MMP9. These docking results identify 3,4-dimethoxy-6,8-dihydroxycoumarin as the compound with the most consistently favorable docking profile across the selected targets.

Table 3. Predicted binding energies of the selected *Ricinus communis* phytochemicals obtained by molecular docking.

Protein	Compound	Docking score (kcal/mol)	Hydrogen bond interactions	Other key interactions
PTGS2 (PDB ID: 5IKR)	3,4-Dimethoxy-6,8-dihydroxycoumarin	-7.1	SER (A:530)	LEU (A:352), GLY (A:526), VAL (A:349), ALA (A:527), VAL (A:523)
	Ferulic acid	-6.8	TYR (A:385), TYR (A:355)	SER (A:353), ALA (A527), VAL (A:349), LEU (A:352), LEU (A:384), TRP (A:387), MET (A:522)
	p-Coumaric acid	-6.4	TYR (A: 355)	LEU (A:352), ALA (A:527), VAL (A:349)

NFKB1 (PDB ID: 1SVC)	3,4-Dimethoxy-6,8-dihydroxycoumarin	-5.5	GLY (P:55)	LYS (P:80), GLY (P:69), GLY (P:68), HIS (P:67), ARG (P:57), SER (P:243), PHE (P:56),LYS (P:52), PRO (P:71), ARG (P:59)
	Ferulic acid	-4.9	LYS (P:52), SRG (P:59)	PHE (P:56), ARG (P:57)
	p-Coumaric acid	-4.8	LYS (P:52), ARG (P:59)	PHE (P:56), ARG (P:57)
MMP9 (PDB ID: 4WZV)	3,4-Dimethoxy-6,8-dihydroxycoumarin	-6.6	-	LEU (A:187), VAL (A:223), LEU (A:188), GLU (A:227)
	Ferulic acid	-7.9	MET (A:247), ARG (A:249), GLU (A:227)	VAL (A:223), HIS (A:226), LEU (A:188), ALA (A:189),PRO (A:246), TYR (A:245), TYR (A:248), LEU (A:222), LEU (A:243)
	p-Coumaric acid	-7.6	MET (A:247), GLU (A:227)	TYR (A: 245), TYR (A:248), HIS (A:226), VAL (A:223), LEU (A:188), ALA (A:189), PRO (A:246), LEU (A:222)LEU (A:243), ARG (A:249)
STAT3 (PDB ID: 6NUQ)	3,4-Dimethoxy-6,8-dihydroxycoumarin	-4.5	GLY (A:656)	VAL (A:637), ILE (A:659), LYS (A: 658), TYR (A:657), ILE (A:653), TYR (A:640)
	Ferulic acid	-4.4	PRO (A:639), GLU (A:	VAL (A:637)

			638), TYR (A:657)	
	p-Coumaric acid	-4.2	GLN (A:644), TYR (A:657)	VAL (A:637), GLU (A:638)
EGFR (PDB ID: 1M17)	3,4-Dimethoxy-6,8-dihydroxycoumarin	-6.8	GLN (A:767), MET (A:769)	VAL (A:702), ALA (A:719), ASP (A:831), GLU (A:738), LYS (A:721), THR (A:830), MET (A:742), THR (A:766), LEU (A:820), LEU (A:768), GLY (A:772), LEU (A:694)
	Ferulic acid	-6.4	LYS (A:721)	VAL (A:702), MET (A:742), ASP (A:831), GLU (A:738), THR (A:830), LE (A:820), GLN (A:767), ALA (A:719), THR (A:766), LEU (A:768), MET (A:769), LEU (A:694)
	p-Coumaric acid	-6.0	LYS (A:721), GLN (A:767)	VAL (A:702)

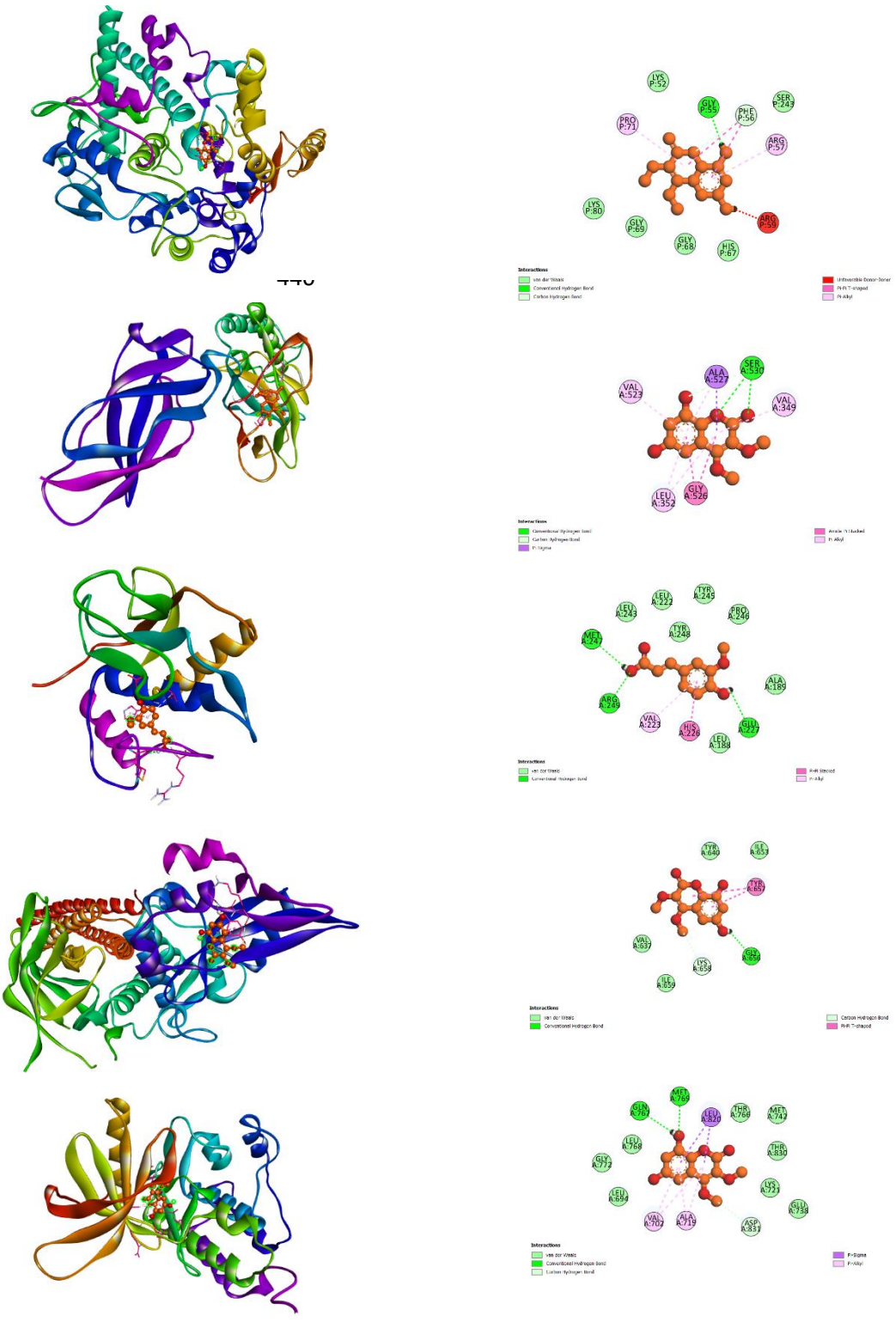


Figure 9. Molecular docking analysis of selected *Ricinus communis* phytochemicals against target proteins. **(A)** PTGS2 vs 3,4-Dimethoxy-6,8-dihydroxycoumarin, **(B)** NFKB1 vs 3,4-Dimethoxy-6,8-dihydroxycoumarin, **(C)** MMP9 vs Ferulic acid, **(D)** STAT3 vs 3,4-Dimethoxy-6,8-dihydroxycoumarin, **(E)** EGFR vs 3,4-Dimethoxy-6,8-dihydroxycoumarin.

2.10. Molecular dynamics simulations

To further examine the dynamic behavior of the top-ranked docked complexes, 25 ns molecular dynamics (MD) simulations were performed for COX-2/PTGS2 with 3,4-dimethoxy-6,8-dihydroxycoumarin, MMP9 with ferulic acid, and EGFR with 3,4-dimethoxy-6,8-dihydroxycoumarin. The trajectories were evaluated using RMSD, RMSF, radius of gyration (Rg), and hydrogen-bond analysis. The RMSD, RMSF, radius of gyration (Rg), and hydrogen-bond profiles are shown in Figure 10, while the main trajectory observations are summarized in Table 4. The COX-2 and 3,4-dimethoxy-6,8-dihydroxycoumarin complex showed an initial increase in RMSD followed by a relatively stable profile, with values remaining below 0.35 nm throughout the simulation. Most residues exhibited low to moderate fluctuations, while higher RMSF values were limited to specific loop regions. The Rg decreased during the early phase of the simulation and subsequently remained stable, indicating maintenance of the overall protein compactness. Hydrogen-bond interactions were also maintained throughout the trajectory.

The MMP9 and ferulic acid complex similarly showed an initial increase in RMSD followed by a relatively stable trajectory, with RMSD remaining below 0.40 nm. The catalytic region displayed comparatively low residue fluctuations, whereas higher flexibility was observed in specific terminal or loop regions. The Rg remained within a narrow range after the initial equilibration period, while hydrogen-bond interactions were maintained throughout the simulation.

The EGFR and 3,4-dimethoxy-6,8-dihydroxycoumarin complex showed somewhat greater conformational variation than the other two complexes. RMSD increased during the middle portion of the simulation, reaching a maximum of approximately 0.41 nm, but subsequently decreased toward the end of the trajectory. The catalytic core remained comparatively less flexible, whereas greater fluctuations were observed toward the terminal regions. The Rg remained relatively stable after the initial phase, and hydrogen-bond interactions persisted throughout the simulation. Overall, all three complexes showed relatively stable trajectories over the 25 ns simulation period. The observed RMSD and Rg profiles remained within relatively narrow ranges after the initial equilibration phase, while residue fluctuations were mainly localized to flexible regions. The persistence of hydrogen-bond interactions further supported the stability of the protein-ligand complexes during the simulated period.

Table 4. Molecular dynamics simulation characteristics of the three selected protein–ligand complexes.

Complex	RMSD range (nm)	RMSF range/major fluctuations (nm)	Rg range (nm)	H-bond range
COX-2 + 3,4-dimethoxy-6,8-dihydroxycoumarin	0.11-0.34	Mostly 0.1-0.2; peaks ~0.73 and 0.52	2.33-2.42	~370-453
MMP9 + ferulic acid	0.05-0.37	Catalytic core <0.10; peaks ~0.48 and 0.38	1.42-1.49	~95-120
EGFR + coumarin	0.05-0.41	Core 0.05-0.15; C-terminal peak ~0.47	1.92-2.02	~185-220

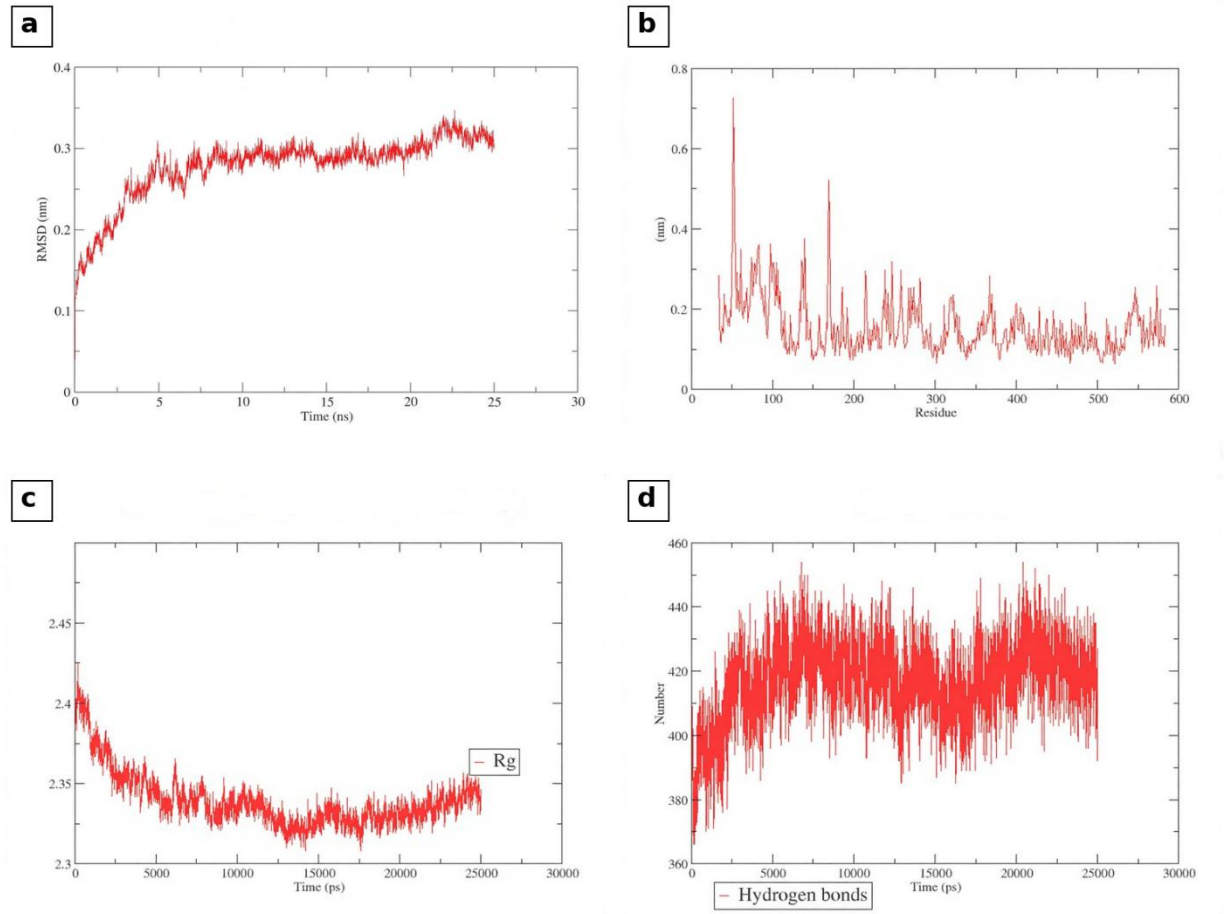


Figure 10. Molecular dynamics simulation of the COX-2 (PTGS2; PDB: 5IKR)-3,4-dimethoxy-6,8-dihydroxycoumarin complex over 25 ns. **(a)** Backbone RMSD as a function of simulation time. **(b)** Per-residue RMSF of the COX-2 backbone. **(c)** Radius of gyration (Rg) of the protein-ligand complex as a function of simulation time. **(d)** Number of intermolecular hydrogen bonds as a function of simulation time. RMSD stabilized below 0.35 nm after initial equilibration, and Rg and hydrogen-bond profiles remained consistently stable throughout the trajectory, indicating a structurally stable complex.

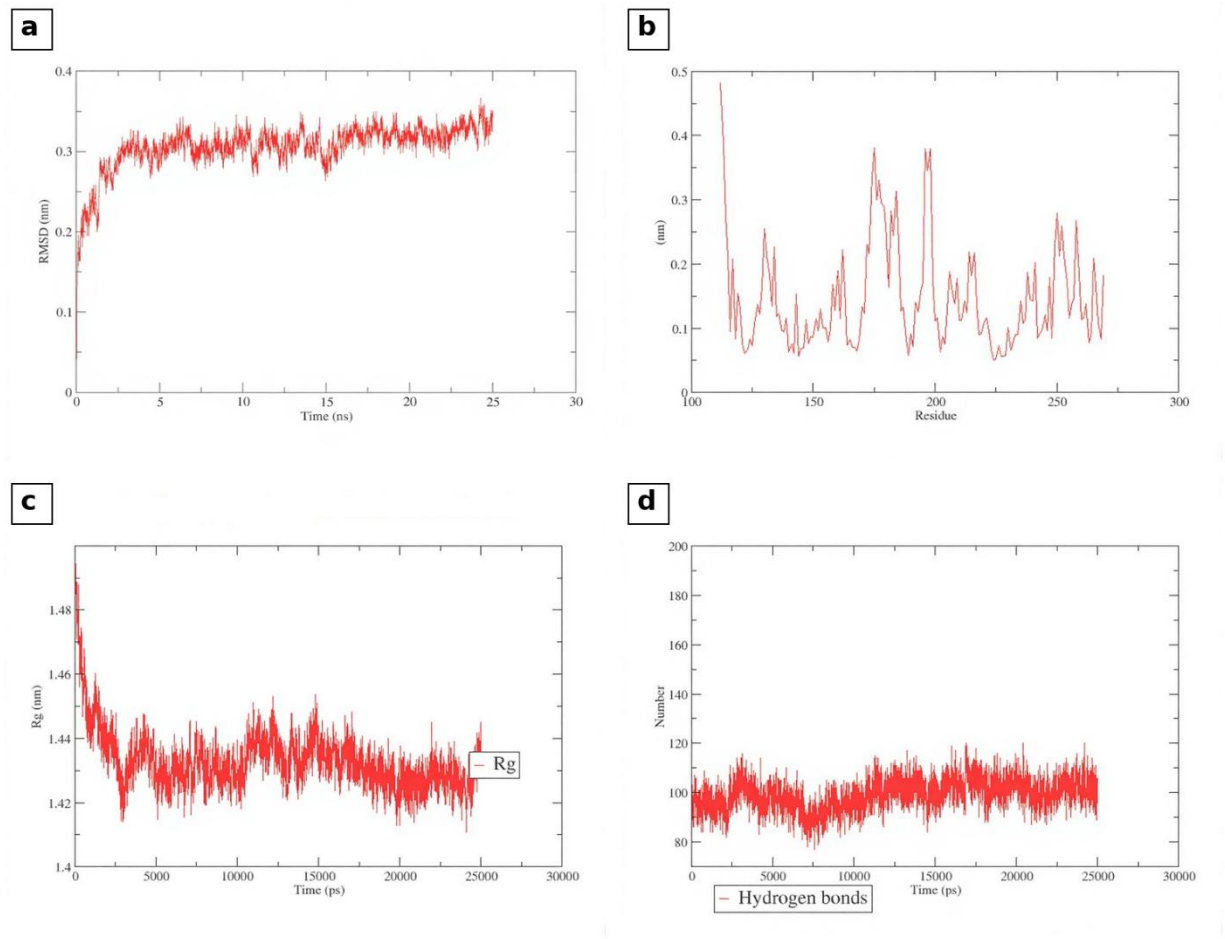


Figure 11. Molecular dynamics simulation of the MMP9 (PDB: 4WZV)-ferulic acid complex over 25 ns. (a) Backbone RMSD as a function of simulation time. (b) Per-residue RMSF of the MMP9) catalytic domain. (c) Radius of gyration (Rg) of the MMP9-ligand complex as a function of simulation time. (d) Number of intermolecular hydrogen bonds as a function of simulation time. RMSD remained below 0.40 nm after equilibration, with low fluctuation across the catalytic core and sustained hydrogen bonding throughout the simulation.

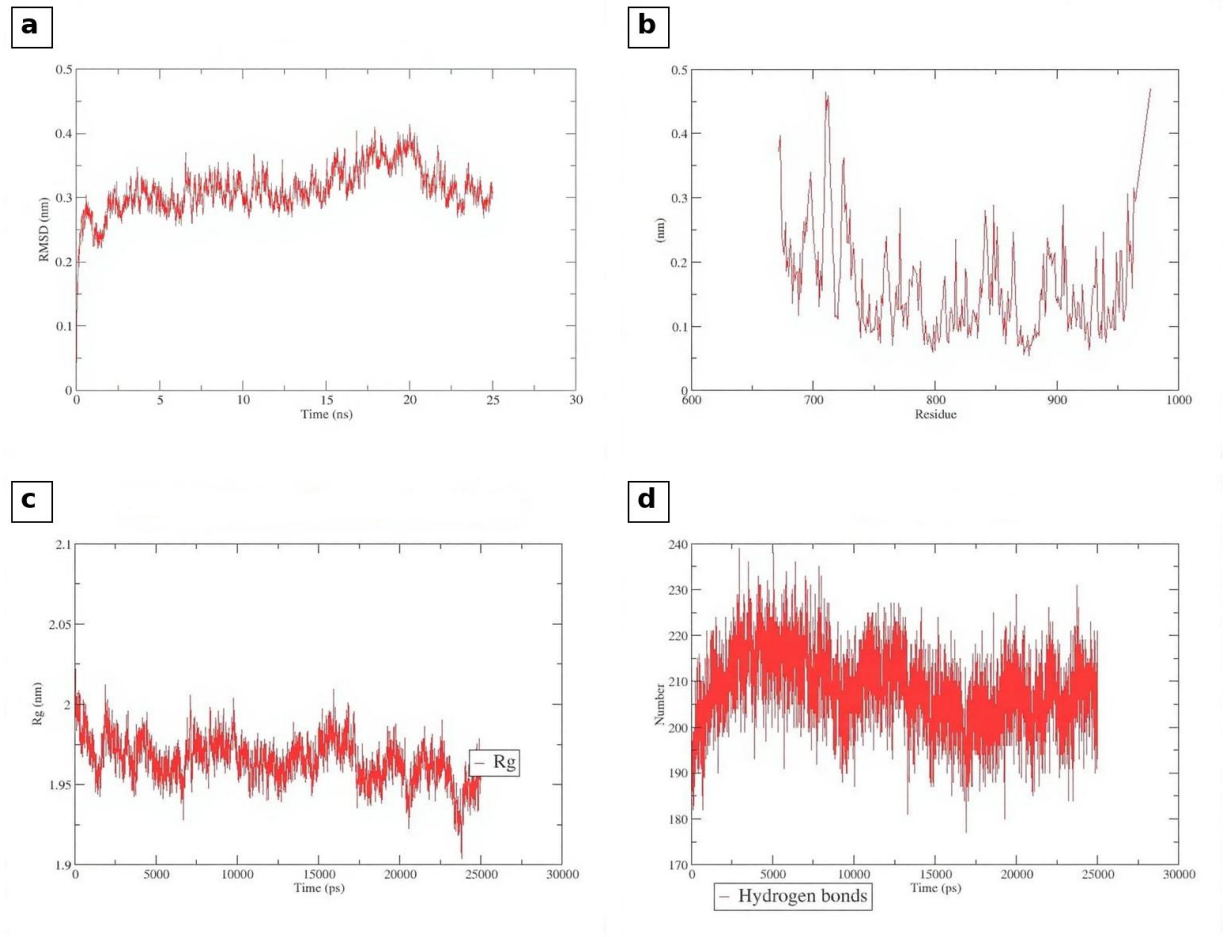


Figure 12. Molecular dynamics simulation of the EGFR (PDB: 1M17)-3,4-dimethoxy-6,8-dihydroxycoumarin complex over 25 ns. (a) Backbone RMSD as a function of simulation time. (b) Per-residue RMSF of the EGFR kinase domain. (c) Radius of gyration (Rg) of the EGFR-ligand complex as a function of simulation time. (d) Number of intermolecular hydrogen bonds as a function of simulation time. RMSD showed a transient increase to ~0.41 nm between 16-20 ns before re-stabilizing, while Rg and hydrogen-bond interactions remained within a stable, compact range throughout the trajectory.

3. Discussion

Dental pain associated with pulpitis and odontogenic inflammation arises from the interaction of microbial challenge, tissue injury, inflammatory mediator release, and sensitization of peripheral sensory pathways. In this setting, inflammatory signaling within the dental pulp is closely linked to the development and persistence of nociceptive responses. NF-κB, cytokine signaling, prostaglandin production, and tissue-remodeling processes have all been implicated in pulpal inflammation and therefore provide biologically relevant contexts in which potential anti-inflammatory phytochemicals may be investigated [15]. *Ricinus communis* L. has a long history of medicinal use and has demonstrated antinociceptive and anti-inflammatory effects in preclinical studies, although the molecular basis of these effects and the constituents responsible remain incompletely characterized [16]. The present study therefore used an integrated computational approach to prioritize *R. communis* phytochemicals and explore their possible relationships with molecular processes relevant to dental pain. Rather than identifying a single definitive mechanism, the findings suggest a network of candidate compound target interactions involving inflammatory and signaling pathways that may warrant experimental investigation.

The prioritization of 3,4-dimethoxy-6,8-dihydroxycoumarin, ferulic acid, and p-coumaric acid is of particular interest because two of these compounds already have independent evidence of anti-inflammatory activity. Ferulic acid has been reported to modulate several inflammatory pathways, including NF-κB and MAPK signaling, and to reduce the production of inflammatory mediators in experimental models [17, 18]. Similarly, p-coumaric acid has been shown to suppress inflammatory responses accompanied by reductions in NF-κB and COX-2 expression in experimental systems [19]. These observations do not demonstrate that either compound acts against dental pain, but they provide pharmacological context for their prioritization in the present study. The findings also complement previous reports of antinociceptive activity of *R. communis* leaf extract in chemical, thermal, and formalin-induced models of pain [16]. Thus, the present analysis provides a possible molecular framework through which some of the previously reported biological activities of the plant could be investigated at the level of individual constituents.

The predicted target network further suggests that the potential relevance of these compounds may extend beyond a single inflammatory mediator. PTGS2, NFKB1, STAT3, EGFR, and MMP9 were prioritized as central nodes, placing them within biological processes that have varying degrees of relevance to pulpal inflammation. NF-κB is particularly well established in dental inflammatory responses. Experimental stimulation of human dental pulp stem cells with TNF-α and lipopolysaccharide activates the IKK/NF-κB pathway and induces expression of the NF-κB-dependent chemokine IL-8, demonstrating the responsiveness of pulp-derived cells to inflammatory stimuli through this pathway [15]. IL-17 provides another relevant connection. Increased IL-17 expression has been reported in human pulpitis, while experimental exposure of human dental pulp fibroblasts to IL-17 increases inflammatory chemokines including IL-6 and IL-8 [20]. These findings provide biological support for the IL-17 and NF-κB-related associations suggested by the present network analysis. Importantly, however, pathway enrichment and target prediction cannot establish whether the prioritized compounds activate or inhibit these pathways; they identify relationships that require experimental clarification.

The predicted involvement of PTGS2 is also relevant to the relationship between inflammation and nociception. COX-2 contributes to prostaglandin synthesis during inflammatory responses, while prostaglandins are established mediators of peripheral nociceptor sensitization. Accordingly, a predicted association between the selected phytochemicals and PTGS2 provides a plausible link to the inflammatory component of dental pain. This interpretation is further supported by the reported ability of ferulic acid and p-coumaric acid to modulate COX-2-associated inflammatory responses in other experimental models [17, 19]. Nevertheless, the present findings should not be interpreted as evidence of direct COX-2 inhibition. Whether the prioritized compounds inhibit COX-2 enzymatic activity, reduce its expression, or influence prostaglandin production remains to be determined experimentally.

The identification of STAT3 and EGFR alongside NF-κB and PTGS2 suggests that the predicted interactions may involve interconnected signaling processes rather than isolated inflammatory targets. EGFR participates in cellular responses to injury and can regulate downstream signaling through pathways including PI3K-AKT and MAPK [21]. STAT3, meanwhile, is a major mediator of cytokine-responsive transcription and can interact with several inflammatory signaling networks. The enrichment of PI3K-AKT signaling in the present study may therefore reflect broader cellular responses associated with inflammatory stress, survival, and tissue responses rather than a pathway specifically responsible for pain perception. A similar consideration applies to HIF-1 signaling. HIF-1α is stabilized under hypoxic conditions and has been increasingly implicated in the biology of pulpitis, where bacterial and inflammatory stimuli can interact with hypoxia-associated signaling [22]. The enrichment of HIF-1-related processes therefore provides additional biological context for the computational network, but it should not be taken as evidence that the selected compounds directly regulate HIF-1α.

MMP9 represents another potentially relevant but biologically complex target. Increased MMP9 expression has been reported in inflamed human dental pulp compared with healthy pulp, supporting its association with pulpal inflammatory processes [23]. However, its role cannot be interpreted simply as pathogenic because experimental MMP9 deficiency has been associated with larger periapical lesions, indicating that MMP9 may also participate in host responses and tissue remodeling during periapical inflammation [24]. Consequently, the predicted association of the prioritized phytochemicals with MMP9 should be regarded as identification of a candidate regulatory node rather than evidence that MMP9 inhibition would necessarily be beneficial. This distinction is important when interpreting network pharmacology results, because centrality within a disease-associated network does not establish the direction or functional consequence of a compound-target interaction.

The DFT, docking, and molecular dynamics analyses provided complementary evidence for prioritizing specific compound-target relationships. The comparatively favorable electronic profile of 3,4-dimethoxy-6,8-dihydroxycoumarin was consistent with its broader predicted docking profile, whereas the favorable predicted interaction of ferulic acid with MMP9 indicates that target-specific structural complementarity may also contribute substantially to binding. Thus, the DFT descriptors provide useful chemical context but should not be considered direct predictors of protein affinity, which depends on the three-dimensional binding environment and multiple ligand-protein interactions. Molecular docking similarly provides plausible binding modes and relative scoring rather than experimentally determined

affinities; limitations in scoring functions and the treatment of protein flexibility can affect the quantitative interpretation of docking results [25].

The subsequent 25 ns molecular dynamics simulations provided an additional assessment of the selected docked complexes under dynamic conditions. The persistence of the complexes during the simulated trajectories supports the compatibility of the predicted poses with the modeled protein environment, but does not establish experimental binding or target inhibition. MD simulations are dependent on factors including the starting structure, force field, system preparation, and sampling time, and therefore are best interpreted as complementary structural evidence rather than experimental confirmation [26].

Taken together, the agreement between network pharmacology, pathway analysis, DFT, docking, and MD provides a coherent computational basis for prioritizing the identified compound-target relationships. The predicted involvement of PTGS2, NFKB1, STAT3, EGFR, and MMP9 within inflammatory signaling networks is also biologically plausible in light of their reported associations with pulpal inflammation and related tissue responses [15, 20, 23].

Overall, the integrated findings suggest that selected *R. communis* phytoconstituents may interact with interconnected molecular targets relevant to dental inflammation and pain. Among the screened compounds, 3,4-dimethoxy-6,8-dihydroxycoumarin and ferulic acid were prioritized as the most promising candidates based on the combined evidence from network pharmacology, DFT, molecular docking, and molecular dynamics simulations. While these findings do not establish a therapeutic mechanism, they provide a coherent and experimentally testable molecular framework for understanding the potential contribution of *R. communis* constituents to inflammatory and nociceptive processes. Further experimental studies are warranted to determine whether the predicted compound-target interactions translate into measurable pharmacological effects.

4. Methods

4.1 Study design and computational workflow

An integrated *in silico* workflow was used to investigate the potential molecular basis of *Ricinus communis* phytoconstituents in dental pain. Phytochemicals reported from the aerial parts of *R. communis* were collected and curated before sequential drug-likeness, ADMET, and toxicity screening. The prioritized compounds were then subjected to target prediction, and their predicted targets were compared with dental pain associated targets retrieved using "Toothache" and "Pulpitis." Common targets were analyzed by protein protein interaction (PPI) analysis, hub target identification, and GO and KEGG enrichment. A compound target pathway network was also constructed to visualize the main relationships within the predicted network. For structural analysis, the prioritized compounds were geometry optimized using DFT, the resulting optimized structures were used for molecular docking against selected hub targets and MD simulation were further performed.

4.2 Phytochemicals collection and curation

Phytoconstituents reported from the aerial parts of *Ricinus communis* were retrieved from the Indian Medicinal Plants, Phytochemistry and Therapeutics (IMPPAT) database and Dr. Duke's Phytochemical and Ethnobotanical Databases. The records obtained from both sources were compiled into a single dataset to establish the initial phytochemical library for the study.

Duplicate entries were identified and removed to avoid repeated representation of the same compound in subsequent analyses. After removal of duplicate entries, 47 unique phytoconstituents were retained for further computational screening. The chemical structures and SMILES representations were obtained from PubChem where available. For compounds without a corresponding structure in PubChem, the chemical structures were drawn in ChemDraw based on their IUPAC names.

4.3 ADME and Drug likeness screening

The 47 curated *R. communis* phytoconstituents were subjected to an initial in two steps. In the first step, SwissADME was used to assess bioavailability, Lipinski's rule of five, and gastrointestinal absorption [27]. Compounds with a bioavailability score ≥0.55, no Lipinski violations, and high GI absorption were retained for further screening. The compounds that passed the first screening were then analyzed using ADMETlab 3.0 [28]. A drug-likeness (DL) score >0.65 was used to select compounds for the subsequent toxicity and target analyses.

4.5 Toxicity prediction using ProTox

The compounds that passed the ADMETlab 3.0 screening were evaluated for acute toxicity using ProTox 3.0 [29]. The canonical SMILES of each compound were submitted to the platform, and the predicted oral LD_{50} and toxicity class were recorded. The three compounds identified after drug-likeness screening were then taken forward for target prediction and network pharmacology analysis.

4.6 Target prediction of prioritized phytoconstituents

Potential targets of the three prioritized *R. communis* phytoconstituents were predicted using the SwissTargetPrediction web server [30]. The chemical structure of each compound was submitted separately, with *Homo sapiens* selected as the target organism. The predicted human protein targets with a probability score greater than 0 were retained for further analysis.

The target lists obtained for the three compounds were then pooled, and duplicate targets were removed. This resulted in 171 unique predicted targets associated with the prioritized phytoconstituents. These targets were subsequently compared with the targets related to dental pain to identify the common molecular targets for the network pharmacology analysis.

The predicted targets were considered putative compound protein associations and were used as computationally predicted targets rather than experimentally validated interactions.

4.7 Identification of dental pain associated targets

Dental pain-associated targets were retrieved from the GeneCards and Comparative Toxicogenomics Database (CTD) [31]. The terms "Toothache" and "Pulpitis" were used to obtain disease-related targets, covering dental pain and pulp inflammation associated with odontogenic pain. For GeneCards, genes with a Relevance Score ≥10 were retained. For CTD, genes were ranked according to their Inference Score, and the top 20% were selected. The resulting gene lists from both databases were combined, and duplicate entries were removed. A total of 1,909 unique dental pain-associated targets were obtained and used for subsequent comparison with the predicted targets of the prioritized *R. communis* phytoconstituents.

4.8 Identification of common targets

The predicted targets of the three prioritized *R. communis* phytoconstituents were compared with the dental pain associated targets obtained from GeneCards and CTD. The two target sets were intersected to identify proteins shared between the prioritized compounds and dental pain. Venn diagram analysis was used to visualize the overlap between the compound- and disease-

associated targets (Venny2.1) [32]. The resulting common targets were considered potential molecular targets through which the prioritized phytoconstituents may be associated with dental pain and were taken forward for subsequent network pharmacology analyses.

4.9 PPI network construction and hub genes

The 55 common targets identified between the *R. communis* phytoconstituent associated targets and dental pain associated targets were analyzed using the STRING database. *Homo sapiens* was selected as the organism to obtain the corresponding human protein interactions. The interaction data were downloaded from STRING and imported into Cytoscape for network visualization and analysis. Hub targets were identified using the CytoHubba plugin in Cytoscape. The Maximal Clique Centrality (MCC) method was used to rank the nodes according to their connectivity within the PPI network. The five targets with the highest MCC scores were selected as hub targets for subsequent analysis [31].

4.10 GO and KEGG enrichment analysis

GO and KEGG pathway enrichment analyses were carried out for the 55 common targets using ShinyGO0.80. GO analysis was performed for the three categories: Biological Process (BP), Molecular Function (MF), and Cellular Component (CC). KEGG enrichment analysis was performed using the same target set to identify the pathways associated with the common targets. The enriched GO terms and KEGG pathways were evaluated based on the statistical results generated by ShinyGO. The significantly enriched terms and pathways were ranked according to their statistical significance and number of associated targets. The resulting enrichment profiles were used for further interpretation of the biological functions and pathways associated with the common targets [31].

4.11 Compound target pathway network construction

A compound target pathway network was constructed in Cytoscape to visualize the relationships among the prioritized *R. communis* phytoconstituents, their predicted targets, and the enriched pathways. The network was generated by combining the compound target interactions obtained from SwissTargetPrediction with the 55 common targets identified through intersection analysis and the significantly enriched GO terms and KEGG pathways.

The resulting network was visualized in Cytoscape, and the connections among compounds, common targets, and enriched pathways were examined to identify the major compound–target–pathway relationships [31].

4.12. Density functional theory based geometry optimization

Density Functional Theory (DFT) calculations were performed for *Ricinus communis* phytoconstituents (3,4-Dimethoxy-6,8-dihydroxycoumarin, Ferulic acid, and p-Coumaric acid) using the B3LYP functional with the 6-311G basis set in Gaussian 09W. The molecular geometries of the selected compounds were optimized before further calculations. The optimized structures and frontier molecular orbitals were visualized using GaussView 5. The highest occupied molecular orbital (HOMO) and lowest unoccupied molecular orbital (LUMO) were evaluated to characterize the electronic properties of the optimized phytoconstituents. The frontier orbital energies were further used to calculate the HOMO-LUMO energy gap and global electronic descriptors within the conceptual DFT framework, based on the interpretations of Parr and Pearson and Koopmans' theorem [33]. The calculated descriptors included ionization potential, electron affinity, electronegativity, chemical hardness, chemical softness, chemical potential, and electrophilicity index.

The electronic descriptors were calculated from the HOMO and LUMO energies using the following relationships:

1. $Energy\ gap\ (\Delta E) = E_{LUMO} - E_{HOMO}\ (eV)$
2. $Ionization\ Energy\ (I) = -(E_{HOMO})(eV)$
3. $Electron\ affinity\ (A) = -(E_{LUMO})(eV)$
4. $Hardness\ (\eta) = \frac{1-A}{2}\ (eV)$
5. $Softness\ (S) = \frac{1}{\eta}\ (eV)$
6. $Electronegativity\ (\chi) = \frac{1+A}{2}\ (eV)$
7. $Chemical\ potential\ (\mu) = -\chi = -\frac{1+A}{2}\ (eV)$
8. $Electrophilicity\ index\ (\omega) = \frac{\mu^2}{2\eta}\ (eV)$

The optimized three-dimensional structures obtained from the DFT calculations were used as ligand structures for the subsequent molecular docking analysis. Docking was therefore performed with the optimized conformations of the phytoconstituents.

4.13. Molecular docking analysis

The DFT optimized structures of the three prioritized *R. communis* phytoconstituents were subjected to molecular docking against the selected protein targets identified through the network pharmacology analysis. The optimized ligand structures were prepared using Open Babel and converted into the required format for docking. Docking was performed using AutoDock Vina with the prepared protein structures obtained from the Protein Data Bank (PDB). The resulting binding poses and protein ligand interactions were visualized and analyzed using Discovery Studio Visualizer [34].

4.13.1. Selection and preparation of protein targets

Five hub targets identified from the PPI network, namely PTGS2, NFKB1, MMP9, STAT3, and EGFR, were selected for molecular docking based on their network centrality and biological relevance to the processes associated with dental pain. The corresponding experimentally determined protein structures were retrieved from the PDB using the following structures: PTGS2 (5IKR), NFKB1 (1SVC), MMP9 (4WZV), STAT3 (6NUQ), and EGFR (1M17). Protein structures were prepared in Discovery Studio before docking. Water molecules, buffer components, and other non-essential heteroatoms were removed, while the required protein structure was retained. Missing hydrogen atoms were added, and the ionizable residues were assigned appropriate protonation states under physiological conditions. For proteins containing multiple identical chains, chain A was selected for docking. The prepared protein structures were saved in PDB format and then converted to PDBQT format using AutoDock Tools. Polar hydrogen atoms and Kollman united atom charges were assigned during receptor preparation.

4.13.2. Ligand preparation

The molecular structures of the selected compounds were retrieved from the PubChem database in SDF format. For 3,4-dimethoxy-6,8-dihydroxycoumarin, for which a corresponding structure was unavailable in PubChem, the 2D structure was drawn in ChemDraw based on its IUPAC name and subsequently converted to a three-dimensional (3D) structure using Avogadro. All ligand structures were then subjected to DFT-based geometry

optimization. The optimized structures were converted to PDB format and used as ligands for subsequent molecular docking studies.

4.13.3. Definition of docking sites and grid parameters

The docking regions were defined using the binding-site coordinates specified for each protein target. The grid-center coordinates were set as follows: PTGS2 (5IKR): x = 38.961219, y = 2.352688, z = 61.503469 (box dimensions 15 × 15 × 15 Å); NFKB1 (1SVC): x = 35.019154, y = 16.066769, z = 53.911308 (box dimensions 24 × 24 × 24 Å); MMP9 (4WZV): x = 3.233700, y = 8.326300, z = 22.094325 (box dimensions 15 × 15 × 15 Å); STAT3 (6NUQ): x = 13.126458, y = 55.609983, z = 0.109915 (box dimensions 18 × 18 × 18 Å); and EGFR (1M17): x = 22.013690, y = 0.252828, z = 52.794034 (box dimensions 15 × 15 × 15 Å).

4.13.4. Docking

Molecular docking was carried out using AutoDock Vina with the predefined coordinates of the binding sites. The exhaustiveness was set to 8, and multiple poses were generated for each compound protein pair. The predicted binding affinity was recorded in kcal/mol, and the pose with the lowest binding energy was selected for further analysis. The selected poses were examined to assess their position within the binding pocket and their interactions with the surrounding amino acid residues.

4.14. Molecular Dynamics Simulation

Molecular dynamics (MD) simulations were performed to further evaluate the conformational stability and binding persistence of the top ranked protein ligand complexes obtained from molecular docking. The simulations were carried out using the WEBGRO Macromolecular Simulations online server (https://simlab.uams.edu/ProteinWithLigand/index.html) [35]. Three docked complexes were selected for MD analysis based on their docking scores: COX-2 (PTGS2; PDB ID: 5IKR) complexed with 3,4-dimethoxy-6,8-dihydroxycoumarin, MMP9 (PDB ID: 4WZV) complexed with ferulic acid, and EGFR (PDB ID: 1M17) complexed with 3,4-dimethoxy-6,8-dihydroxycoumarin.

For each complex, the GROMOS96 43a1 force field and SPC water model were used. The protein-ligand complexes were placed in a triclinic simulation box and solvated with water. The systems were neutralized with NaCl, and additional NaCl was added to obtain a final salt concentration of 0.15 M. Before the production run, energy minimization was performed using the steepest-descent algorithm for 5000 steps to remove unfavorable contacts and obtain energetically favorable starting configurations. The minimized systems were subsequently equilibrated under NVT/NPT conditions at 300 K and 1.0 bar. Following equilibration, each system was subjected to a 25 ns MD simulation using the leap-frog integration algorithm, with approximately 5000 trajectory frames recorded for each simulation. The trajectories obtained from the MD simulations were analyzed using root mean square deviation (RMSD), root mean square fluctuation (RMSF), and hydrogen bond analysis to assess the conformational stability, residue-level flexibility, and persistence of protein-ligand interactions throughout the simulation period.

5. Limitation of the study

The present study is computational in nature and therefore provides predictive rather than experimental evidence for the proposed compound-target relationships. Molecular docking was used to estimate probable binding preferences and prioritize compounds and targets for further

investigation; however, docking scores do not necessarily translate into actual binding affinity or biological potency. Similarly, the 25 ns molecular dynamics simulations provide information on the stability of the predicted complexes within the applied simulation conditions, but the relatively short simulation period and limitations of the selected force field cannot fully reproduce the complexity and timescale of protein-ligand interactions in biological systems. ADME and toxicity predictions were also used as early stage screening tools and should be regarded as approximations rather than substitutes for experimental pharmacokinetic, metabolic, and cytotoxicity assessment. In addition, the network pharmacology and pathway analyses are dependent on available databases and prediction algorithms and therefore may not capture all biologically relevant interactions. These limitations can be addressed through *in vitro* enzyme inhibition and binding assays, dental pulp cell based studies, cytokine and inflammatory mediator profiling, pharmacokinetic and cytotoxicity studies, and ultimately appropriate *in vivo* models. Such experimental validation will be essential to determine whether the computationally prioritized *R. communis* phytoconstituents exert the predicted molecular and antinociceptive effects.

6. Conclusion

This study provides an integrated computational framework for exploring the molecular basis of *Ricinus communis* in dental pain. Sequential screening prioritized 3,4-dimethoxy-6,8-dihydroxycoumarin, ferulic acid, and p-coumaric acid, with PTGS2, NFKB1, STAT3, EGFR, and MMP9 emerging as key candidate targets within interconnected inflammatory pathways. DFT, molecular docking, and molecular dynamics further prioritized 3,4-dimethoxy-6,8-dihydroxycoumarin and ferulic acid based on their predicted structural and dynamic interactions with selected targets. Collectively, these findings suggest a multi-target molecular basis for the potential anti-inflammatory and antinociceptive activity of selected *R. communis* constituents. Although the findings remain computational and require experimental validation, they provide a focused and testable basis for subsequent pharmacological investigation of these phytochemicals in dental inflammation and pain.

References

1. Alves-Costa, S., M. Romandini, and G.G. Nascimento, *Lip and oral cancer, caries and other oral conditions: estimates from the 2021 global burden of disease study and projections up to 2050.* Journal of Periodontal Research, 2025. **60**(6): p. 544-558.
2. Bernabe, E., et al., *Trends in the global, regional, and national burden of oral conditions from 1990 to 2021: A systematic analysis for the Global Burden of Disease Study 2021.* The Lancet, 2025. **405**(10482): p. 897-910.
3. Delgado-Pérez, V.J., et al., *Epidemiological and oral public health aspects of dental pain: A narrative review.* Cureus, 2024. **16**(12).
4. Teoh, L., *Managing acute dental pain without codeine.* Australian Prescriber, 2020. **43**(2): p. 64.
5. Graumlich, J.F., *Preventing gastrointestinal complications of NSAIDs: risk factors, recent advances, and latest strategies.* Postgraduate Medicine, 2001. **109**(5): p. 117-128.

6. Green, V.G., et al., *Evidence-based clinical practice guidelines for the management of acute dental pain.* The American journal of emergency medicine, 2024. **89**: p. 247.
7. Khan Marwat, S., et al., *Ricinus cmmunis: Ethnomedicinal uses and pharmacological activities.* Pakistan Journal of Pharmaceutical Sciences, 2017. **30**(5): p. 1815.
8. Ribeiro, P.R., R.D. de Castro, and L.G. Fernandez, *Chemical constituents of the oilseed crop Ricinus communis and their pharmacological activities: A review.* Industrial Crops and Products, 2016. **91**: p. 358-376.
9. Gupta, R., A.K. Chaudhary, and R. Sharma, *Analgesic and anti-inflammatory potential of Ricinus communis Linn.: evidence from pharmacology to clinical studies.* Current Pharmacology Reports, 2024. **10**(1): p. 27-67.
10. Salmaso, V. and S. Moro, *Bridging molecular docking to molecular dynamics in exploring ligand-protein recognition process: An overview.* Frontiers in Pharmacology, 2018. **9**: p. 923.
11. Śledź, P. and A. Caflisch, *Protein structure-based drug design: from docking to molecular dynamics.* Current opinion in structural biology, 2018. **48**: p. 93-102.
12. Kanehisa, M., et al., *KEGG: Biological systems database as a model of the real world.* Nucleic Acids Research, 2025. **53**(D1): p. D672-D677.
13. Kanehisa, M. and S. Goto, *KEGG: Kyoto encyclopedia of genes and genomes.* Nucleic Acids Research, 2000. **28**(1): p. 27-30.
14. Kanehisa, M., *Toward understanding the origin and evolution of cellular organisms.* Protein Science, 2019. **28**(11): p. 1947-1951.
15. Chang, J., et al., *NF-κB activation in human dental pulp stem cells by TNF and LPS.* Journal of Dental Research, 2005. **84**(11): p. 994-998.
16. Taur, D.J., et al., *Antinociceptive activity of Ricinus communis L. leaves.* Asian Pacific Journal of Tropical Biomedicine, 2011. **1**(2): p. 139-141.
17. Jacobo-Velázquez, D.A., *Ferulic acid: Mechanistic insights and multifaceted applications in metabolic syndrome, food preservation, and cosmetics.* Molecules, 2025. **30**(18): p. 3716.
18. Zhai, Y., et al., *Ferulic acid: A review of pharmacology, toxicology, and therapeutic effects on pulmonary diseases.* International Journal of Molecular Sciences, 2023. **24**(9): p. 8011.
19. Moon, H.-R. and J.-M. Yun, *p-Coumaric acid modulates cholesterol efflux and lipid accumulation and inflammation in foam cells.* Nutrition Research and Practice, 2024. **18**(6): p. 774-792.
20. Xiong, H., L. Wei, and B. Peng, *IL-17 stimulates the production of the inflammatory chemokines IL-6 and IL-8 in human dental pulp fibroblasts.* International Endodontic Journal, 2015. **48**(6): p. 505-511.
21. Carpenter, G., *The EGF receptor: A nexus for trafficking and signaling.* Bioessays, 2000. **22**(8): p. 697-707.
22. Shao, L., et al., *The roles and molecular mechanisms of HIF-1α in pulpitis.* Journal of Dental Research, 2025. **104**(7): p. 715-724.
23. Tsai, C.-H., et al., *The upregulation of matrix metalloproteinase-9 in inflamed human dental pulps.* Journal of Endodontics, 2005. **31**(12): p. 860-862.

24. Wan, C., et al., *MMP9 deficiency increased the size of experimentally induced apical periodontitis.* Journal of Endodontics, 2014. **40**(5): p. 658-664.
25. Huang, S.-Y., S.Z. Grinter, and X. Zou, *Scoring functions and their evaluation methods for protein-ligand docking: Recent advances and future directions.* Physical Chemistry Chemical Physics, 2010. **12**(40): p. 12899-12908.
26. Grewal, S., et al., *Molecular dynamics simulations: Insights into protein and protein ligand interactions.* Advances in Pharmacology, 2025. **103**: p. 139-162.
27. Daina, A. and V. Zoete, *Application of the SwissDrugDesign online resources in virtual screening.* International Journal of Molecular Sciences, 2019. **20**(18): p. 4612.
28. Fu, L., et al., *ADMETlab 3.0: an updated comprehensive online ADMET prediction platform enhanced with broader coverage, improved performance, API functionality and decision support.* Nucleic Acids Research, 2024. **52**(W1): p. W422-W431.
29. Banerjee, P., et al., *ProTox 3.0: A webserver for the prediction of toxicity of chemicals.* Nucleic Acids Research, 2024: p. gkae303.
30. Saleem, M., et al., *Network pharmacology and multitarget analysis of Nigella sativa in the management of diabetes and obesity: a computational study.* Journal of Biomolecular Structure and Dynamics, 2024. **42**(9): p. 4800-4816.
31. Chen, J., et al., *Network pharmacology, molecular docking, and molecular dynamics simulations to explore the effects of sinomenine on thyroid dysfunction.* Scientific Reports, 2025. **15**(1): p. 39084.
32. Nirmalkar, U., et al., *Network pharmacology and molecular docking approaches to illustrate the potential targets and mechanisms of action of green tea catechins against cataract.* Revista Brasileira de Farmacognosia, 2025. **35**(6): p. 1309-1322.
33. Rampadarath, A., et al., *Molecular bioprospection of Helianthus annuus L. (sunflower) cypselae for antidiabetic therapeutics through network pharmacology, density functional theory and molecular dynamics simulation.* South African Journal of Botany, 2023. **162**: p. 72-95.
34. Ahmed, M.Z., et al., *In silico molecular docking analysis of limonene with the fat mass and obesity-associated protein by using autodock vina.* Sci J Informatics, 2021. **8**: p. 154-160.
35. Wahono, C.S., et al., *Exploring the potential of phytoconstituents from Phaseolus vulgaris L against CXC motif chemokine receptor 4 (CXCR4): a bioinformatic and molecular dynamic simulations approach.* Egyptian Journal of Medical Human Genetics, 2024. **25**(1): p. 52.

Acknowledgements
The author sincerely thanks Ongoing Research Funding Program, (ORF-2026-1431), King Saud University, Riyadh, Saudi Arabia for funding this research.

Author Contributions Statement
Sultan Aati: Writing – review & editing, Project administration, Funding acquisition, Conceptualization. Muhammad Ahsan Raza: Writing – original draft, Conceptualization, Methodology, Software, Visualization, Formal analysis, Data curation. Kashif-ur-Rehman Khan: Writing – review & editing, Supervision, Conceptualization. Mohammed Alshehri: Formal analysis, Review & editing. Omar Algeel: Visualization, Review & editing. Obaid Alshahrani: Writing – review & editing. Bilal Ahmad Ghalloo: Methodology, Review & editing. Hanan Aati: Conceptualization, Review & editing.

Data availability
All data generated or analyzed during this study are included in this published article and its supplementary information files.

Funding
This work is funded by Ongoing Research Funding Program, (ORF-2026-1431), King Saud University, Riyadh, Saudi Arabia for funding this research.

Additional Information

Competing interests
The authors declare no financial and non-financial competing interests.

Consent for publication
The KEGG pathway maps (Figure 6A-C) used in this article have been authorized by the KEGG database under written permission (Permission ID: 263062). The permission document has been submitted along with the manuscript.

Legends

Figure Legends

Figure 1. Chemical structures of the prioritized compounds identified in *Ricinus communis*: **(1)** 3,4-Dimethoxy-6,8-dihydroxycoumarin, **(2)** Ferulic acid, and **(3)** p-Coumaric acid

Figure 2. Venn diagram showing the intersection of targets associated with dental pain and prioritized compounds.

Figure 3. PPI network and hub gene identification. The PPI network consisted of 55 common targets with 401 interactions.

Figure 4. Hub genes identified from the PPI network using the MCC algorithm. The five top ranked hub genes were PTGS2, NFKB1, MMP9, STAT3 and EGFR.

Figure 5. Gene Ontology and KEGG pathway enrichment analysis of the common targets. **(A)** KEGG pathway enrichment analysis showing the significantly enriched pathways associated

with the common targets, **(B)** Biological Process (BP) enrichment analysis **(C)** Cellular Component (CC) enrichment analysis and **(D)** Molecular Function (MF) enrichment analysis

Figure 6A. KEGG based visualization of the IL-17 signaling pathway showing predicted targets of *Ricinus communis* phytoconstituents. Pathway map generated using Pathview, with nodes highlighted in red indicating hub/network target genes identified through the network pharmacology analysis (NF-κB, MAPK3/ERK, GSK3β, CXCL2, MMP1, and MMP9).

Figure 6B. KEGG-based visualization of the PI3K-AKT signaling pathway showing predicted targets of *Ricinus communis* phytoconstituents. Pathway map generated using Pathview, with red nodes denoting network hub genes (RTK, ERK, GSK3, NF-κB, and Mcl-1) mapped onto the reference pathway.

Figure 6C. KEGG-based visualization of the HIF-1 signaling pathway showing predicted targets of *Ricinus communis* phytoconstituents. Pathway map generated using Pathview, with red nodes indicating network hub genes (RTK, ERK, STAT3, NF-κB, iNOS, and LDHA) overlaid on the reference pathway.

Figure 7. Compound target pathway network of the bioactive constituents of *Ricinus communis* against dental pain targets. Network constructed and visualized in Cytoscape. Yellow diamond nodes represent the three bioactive compounds (ferulic acid, p-coumaric acid, and 3,4-dimethoxy-6,8-dihydroxy-coumarin); orange nodes represent their predicted gene targets, with hexagonal nodes denoting targets that map onto one or more enriched KEGG pathways and elliptical nodes denoting targets without direct pathway mapping in this network; green rectangular nodes represent the significantly enriched KEGG signaling pathways (Calcium signaling, IL-17 signaling, Ras signaling, PI3K-AKT signaling, HIF-1 signaling, and AGE-RAGE signaling in diabetic complications). Edges connect each compound to its predicted targets and each target to its associated pathway(s), illustrating the multi-compound, multi-target, multi-pathway pharmacological basis of *Ricinus communis* against dental pain.

Figure 8. DFT-optimized molecular structures and corresponding HOMO and LUMO distributions of the selected *Ricinus communis* phytochemicals. **(A)** 3,4-dimethoxy-6,8-dihydroxycoumarin, **(B)** ferulic acid, and **(C)** p-coumaric acid.

Figure 9. Molecular docking analysis of selected *Ricinus communis* phytochemicals against target proteins. **(A)** PTGS2 vs 3,4-Dimethoxy-6,8-dihydroxycoumarin, **(B)** NFKB1 vs 3,4-Dimethoxy-6,8-dihydroxycoumarin, **(C)** MMP9 vs Ferulic acid, **(D)** STAT3 vs 3,4-Dimethoxy-6,8-dihydroxycoumarin, **(E)** EGFR vs 3,4-Dimethoxy-6,8-dihydroxycoumarin.

Figure 10. Molecular dynamics simulation of the COX-2 (PTGS2; PDB: 5IKR)-3,4-dimethoxy-6,8-dihydroxycoumarin complex over 25 ns. **(a)** Backbone RMSD as a function of simulation time. **(b)** Per-residue RMSF of the COX-2 backbone. **(c)** Radius of gyration (Rg) of the protein-ligand complex as a function of simulation time. **(d)** Number of intermolecular hydrogen bonds as a function of simulation time. RMSD stabilized below 0.35 nm after initial equilibration, and Rg and hydrogen-bond profiles remained consistently stable throughout the trajectory, indicating a structurally stable complex.

Figure 11. Molecular dynamics simulation of the MMP9 (PDB: 4WZV)-ferulic acid complex over 25 ns. (a) Backbone RMSD as a function of simulation time. (b) Per-residue RMSF of the MMP9) catalytic domain. (c) Radius of gyration (Rg) of the MMP9-ligand complex as a function of simulation time. (d) Number of intermolecular hydrogen bonds as a function of simulation time. RMSD remained below 0.40 nm after equilibration, with low fluctuation across the catalytic core and sustained hydrogen bonding throughout the simulation.

Figure 12. Molecular dynamics simulation of the EGFR (PDB: 1M17)-3,4-dimethoxy-6,8-dihydroxycoumarin complex over 25 ns. (a) Backbone RMSD as a function of simulation time. (b) Per-residue RMSF of the EGFR kinase domain. (c) Radius of gyration (Rg) of the EGFR-ligand complex as a function of simulation time. (d) Number of intermolecular hydrogen bonds as a function of simulation time. RMSD showed a transient increase to ~0.41 nm between 16-20 ns before re-stabilizing, while Rg and hydrogen-bond interactions remained within a stable, compact range throughout the trajectory.

Table Legends

Table 1. *In silico* ADME, drug-likeness, and toxicity profiles of the three prioritized *Ricinus communis* phytoconstituents.

Toxicity Class I: fatal if swallowed (LD50 ≤ 5), Class II: fatal if swallowed (5 < LD50 ≤ 50), Class III: toxic if swallowed (50 < LD50 ≤ 300), Class IV: harmful if swallowed (300 < LD50 ≤ 2000), Class V: may be harmful if swallowed (2000 < LD50 ≤ 5000), Class VI: non-toxic (LD50 > 5000)

Molecular Weight (MW); Gastrointestinal (GI); Drug Likiness (DL)

Table 2. DFT-calculated frontier molecular orbital energies and conceptual density functional theory (CDFT) descriptors of the selected *Ricinus communis* phytochemicals

Table 3. Predicted binding energies of the selected *Ricinus communis* phytochemicals obtained by molecular docking.

Table 4. Molecular dynamics simulation characteristics of the three selected protein–ligand complexes.

Supplementary Files

This is a list of supplementary files associated with this preprint. Click to download.

- Supplementaryfile28.08.2026.docx